Latest Higgs Results from ATLAS

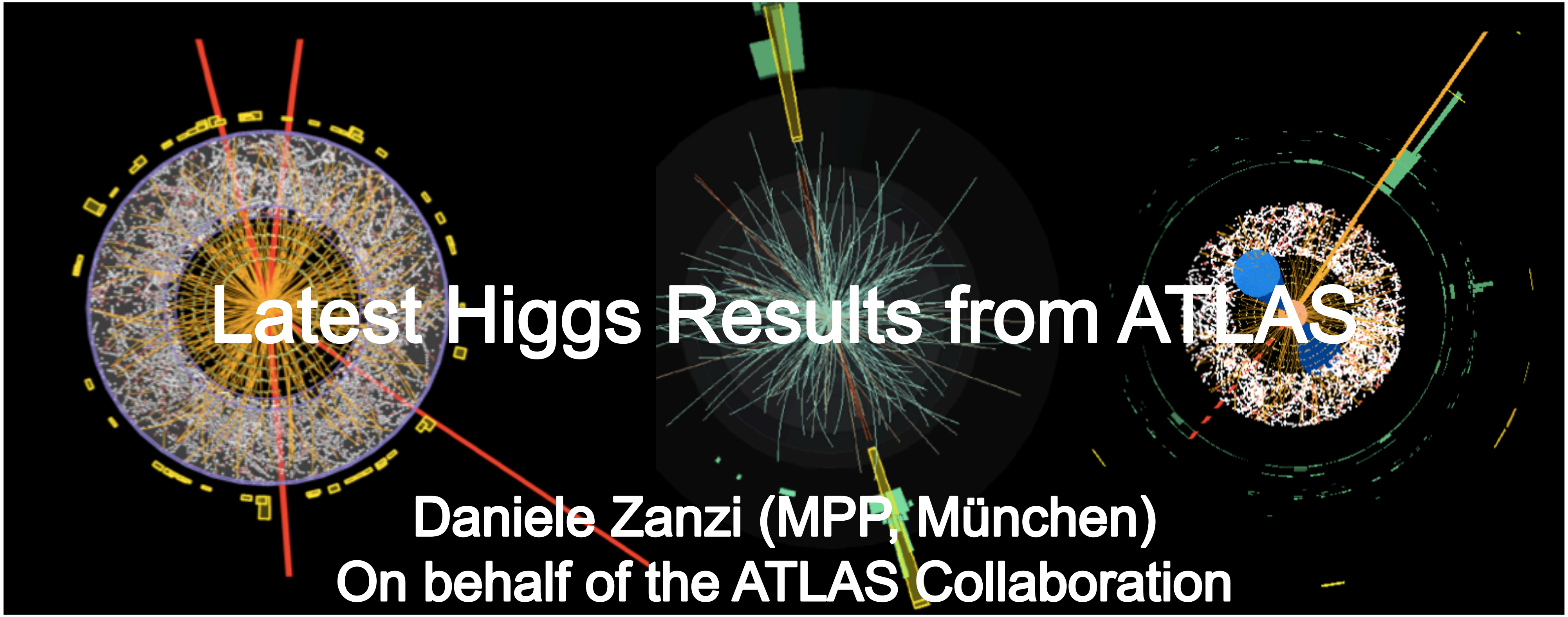

Daniele Zanzi (MPP, München)
On behalf of the ATLAS Collaboration

European Linear Collider Workshop
DESY, Hamburg, 27-31.05.13

ATLAS

FSP 101 ATLAS

Max-Planck-Institut für Physik
(Werner-Heisenberg-Institut)

Introduction

Since the discovery of a new resonance on July 2012:

1. Updates with full 2012 dataset
2. Test of compatibility with SM Higgs boson:
    1. mass
    2. couplings
    3. spin and CP-parity
3. Search for other signals (R. Simoniello's talk)

PLB 716(2012) 1

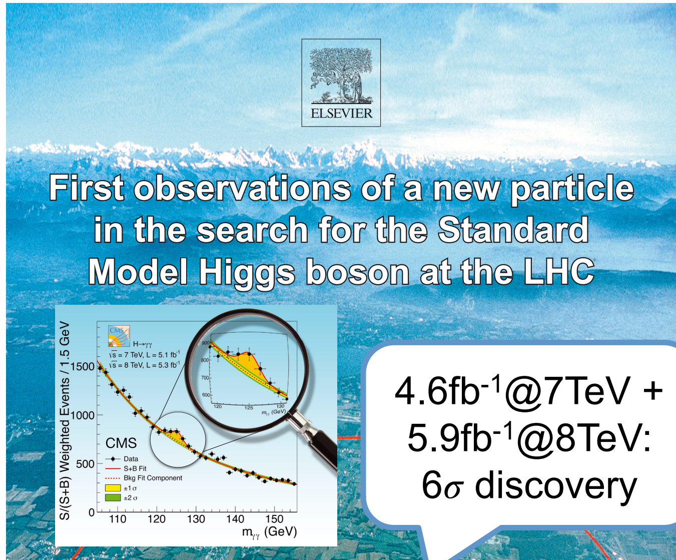

4.6fb^{-1}@7TeV + 5.9fb^{-1}@8TeV: 6σ discovery

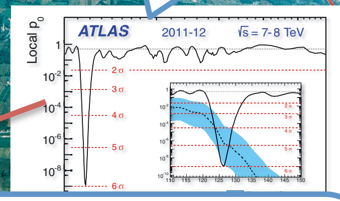

In this talk, latest results on Higgs boson properties based on full 2011+2012 datasets:

- $H\to\gamma\gamma$
- $H\to ZZ$
- $H\to WW$

+ combination

(Fermionic final states not updated yet)

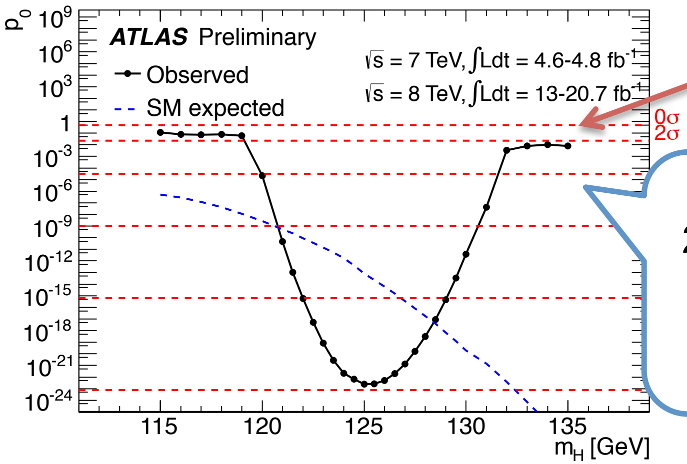

4.6fb^{-1}@7TeV + 20.7fb^{-1}@8TeV: 10σ!!
$H\to 4l$: >6σ
$H\to\gamma\gamma$: >7σ
$H\to WW$: 3.8σ

LHC and ATLAS performance

1. Excellent LHC and ATLAS performances!!
2. ~90% of delivered collisions used by physics analyses
3. Pile-up higher than design value (critical for trigger, computing, object reconstruction)

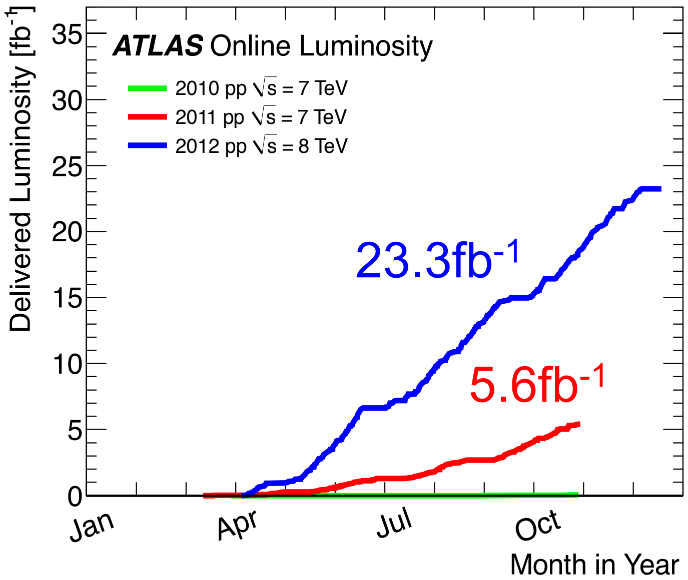

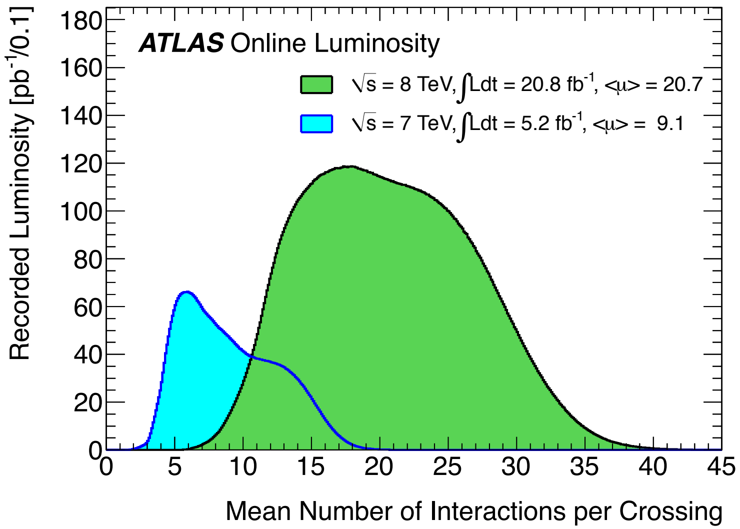

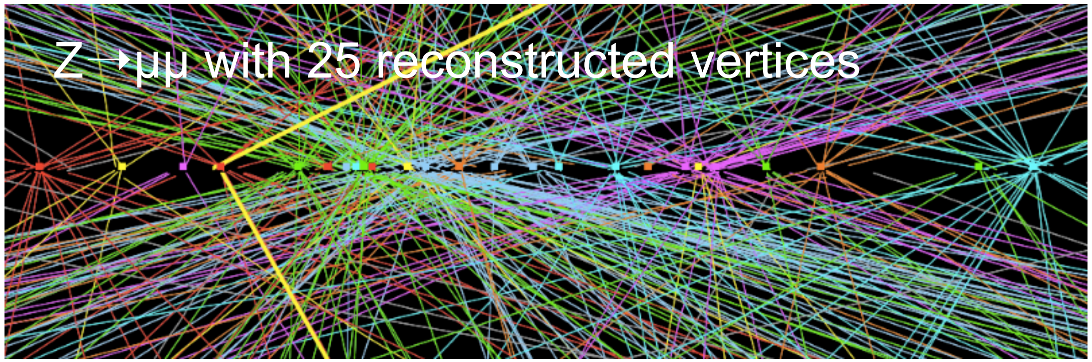

SM Higgs boson @LHC

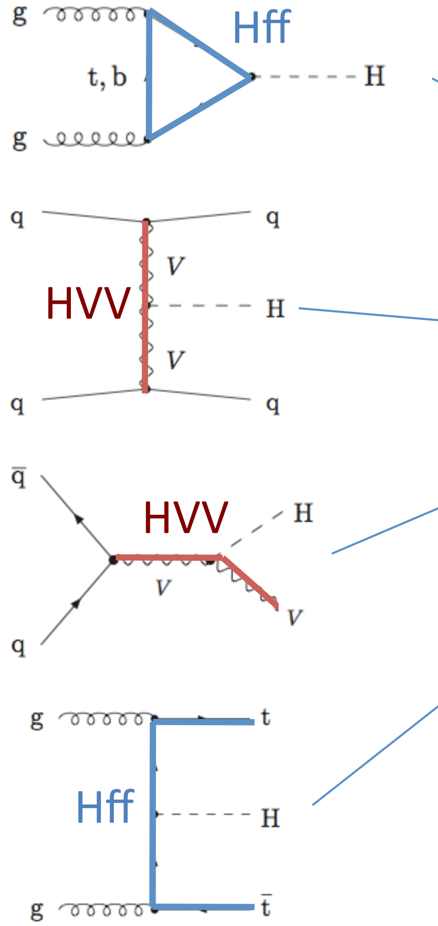

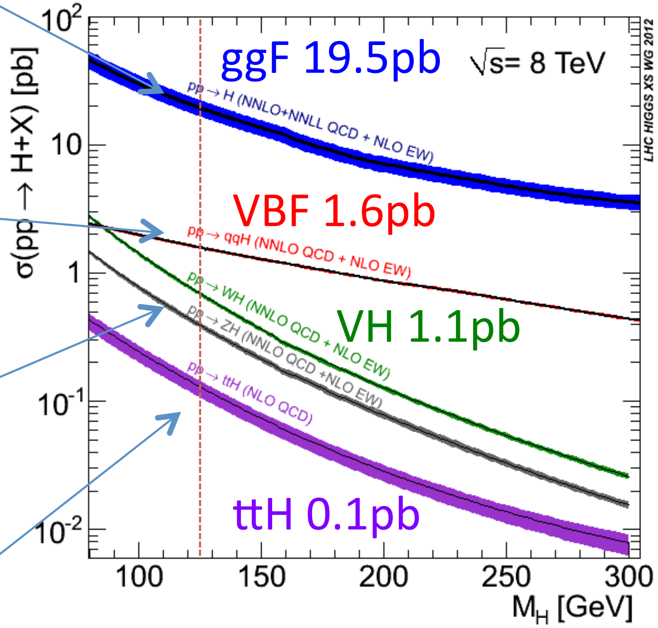

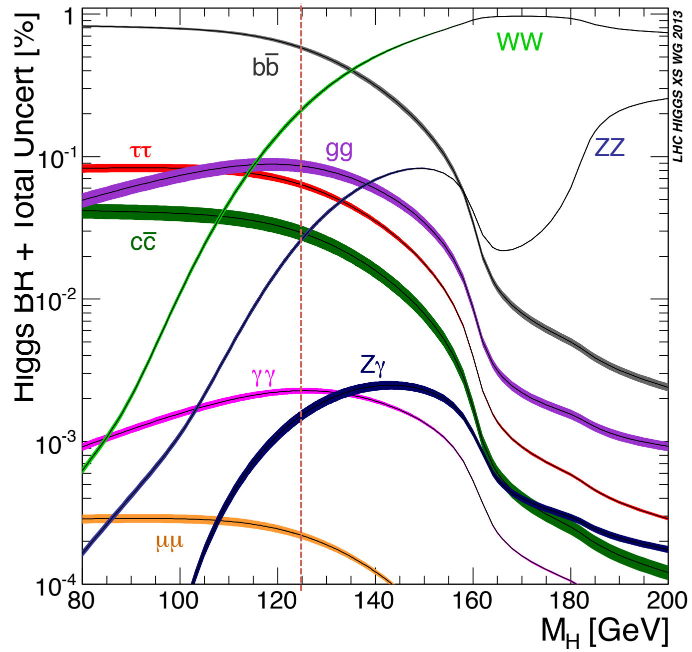

Searches span most of the final states and are optimized for single production modes in order to fully characterize the new boson

Mass & signal strength

$H \rightarrow \gamma\gamma$

ATLAS-CONF-2013-012

1. 2 isolated high-p_T photons (E_T>40,30 GeV)
2. Background extrapolated from side-bands in data
3. Data-driven background decomposition: $\gamma\gamma$ 75%, γj 22%, jj 3%
4. Mass resolution ~1.7GeV at m_H=126.5GeV, very stable wrt pile-up

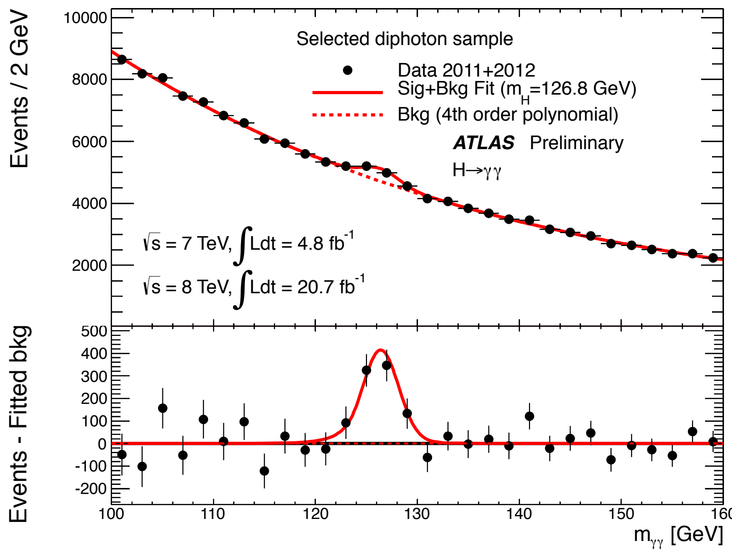

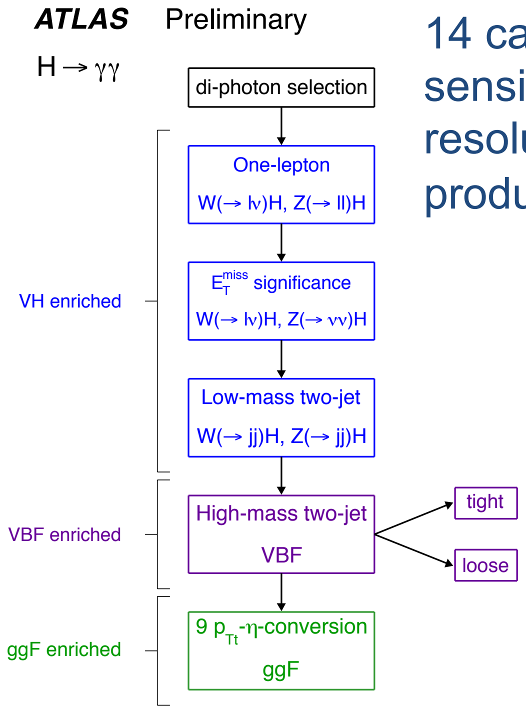

14 categories to increase signal sensitivity (different S/B and mass resolution) and to enhance single production modes (no pure region)

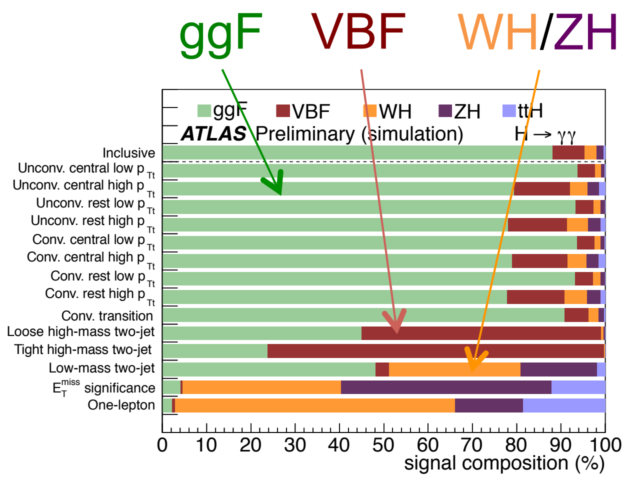

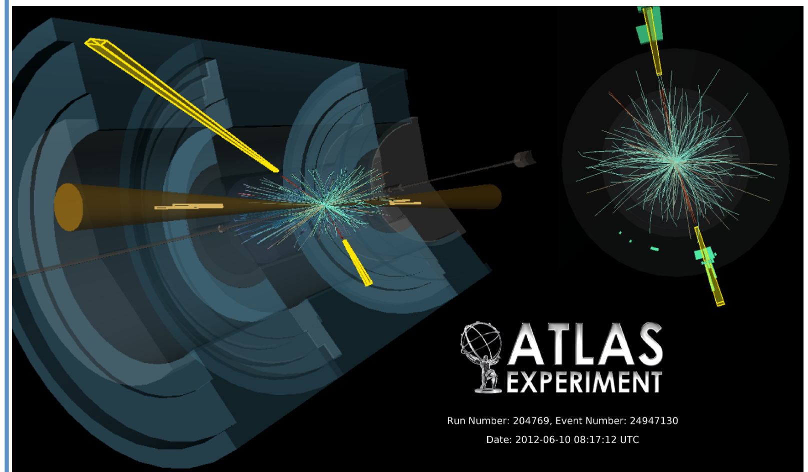

H→γγ: Mass & signal strength

ATLAS-CONF-2013-012

1. Best-fit mass: 126.8±0.2(stat)±0.7(syst) GeV
   dominated by photon energy scale uncertainty
2. Observed(Exp.) significance at 126.5 GeV:
   $7.4\sigma(4.1\sigma)$
3. Signal strength at 126.8 GeV:
   $1.65\pm0.24(\mathrm{stat})^{+0.25}_{-0.18}(\mathrm{syst})$
   2.3σ from the SM hypothesis

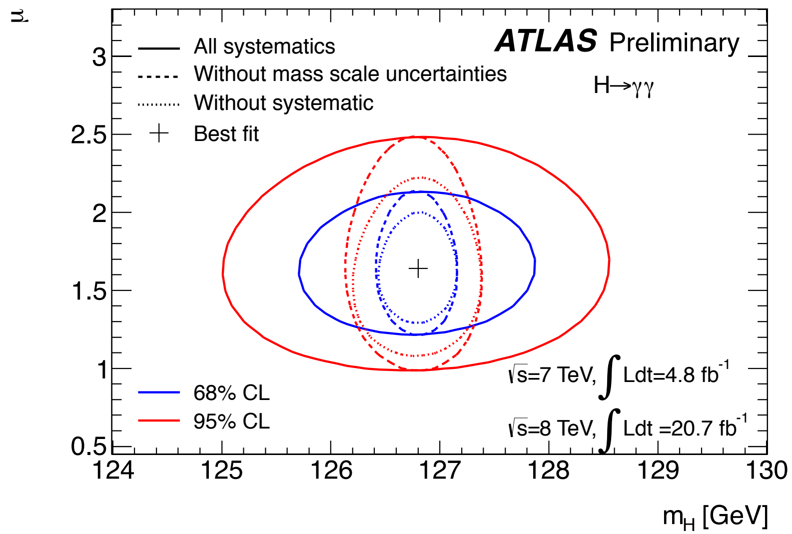

2σ excess observed for the VBF production mode alone for m_H = 126.8 GeV

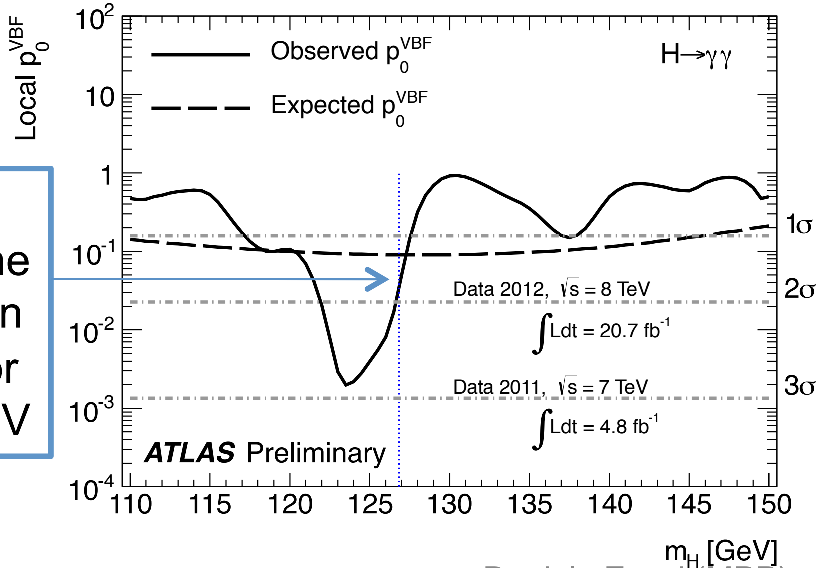

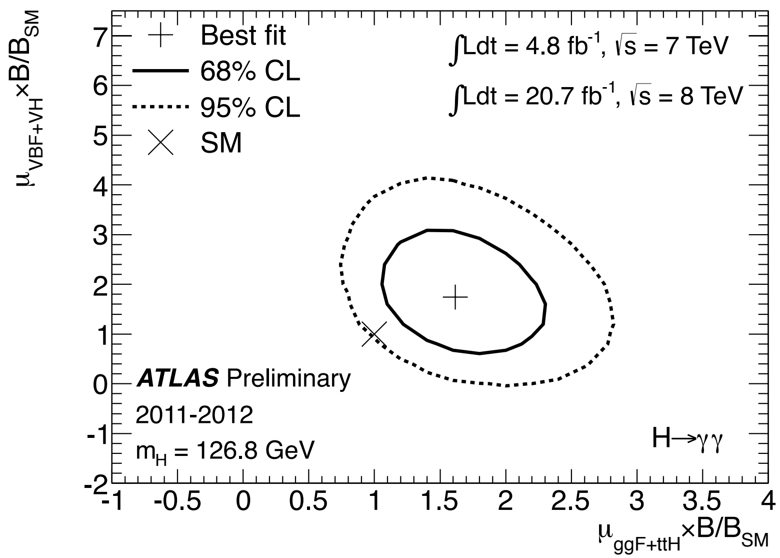

$H \to ZZ^{(*)} \to 4l$

ATLAS-CONF-2013-013

1. 2 OS SF isolated lepton pairs (p_T>20,15, 10, 7(6) GeV)
2. Clean signature, high lepton ID efficiency needed (after full selection ε_{event}~40/20% 4μ/4e)
3. Mass resolution ~1.6-2.4 GeV at m_H=125GeV
4. Irreducible background $ZZ^{(*)}$ from MC, reducible Z+jets and top from control regions in data
5. Syst on lepton reco/ID eff and on energy/momentum resolution (determined using Z, Υ and J/ψ samples)
6. Categorization in VBF/VH/ggF-like events

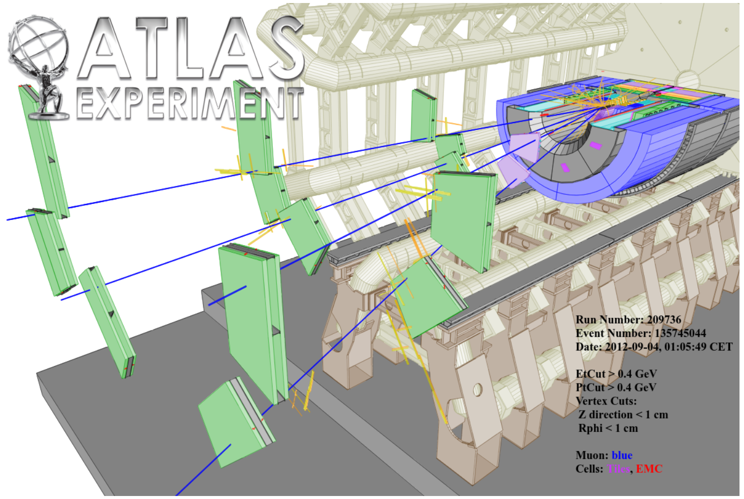

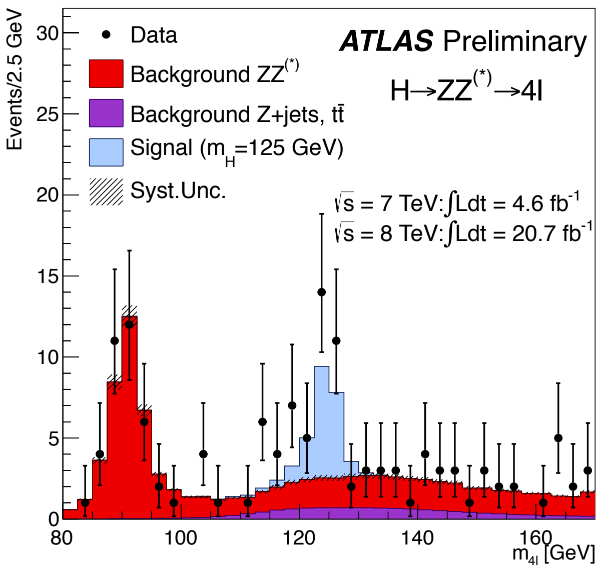

m_{4l} range [GeV]	[120-130]	>160
Observed Events	32	376
Exp. SM signal (m_H=125GeV)	15.9±2.1	
Exp. Bkg	11.1±1.3	348±26

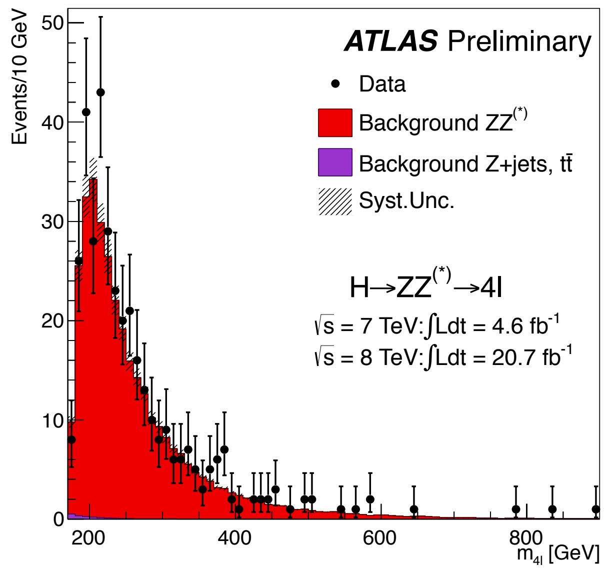

$H \rightarrow ZZ^{(*)} \rightarrow 4l$: Mass & signal strength

ATLAS-CONF-2013-013

1. Best-fit mass: $124.3^{+0.6}_{-0.5}(\text{stat})^{+0.5}_{-0.3}(\text{syst})$ GeV dominated by statistical error, systematic error mainly from energy/momentum scale uncertainties
2. Observed(Exp.) significance at 124.3 GeV: $6.6\sigma(4.4\sigma)$
3. Signal strength at 124.3 GeV: $1.7^{+0.5}_{-0.4}$
4. $\mu_{\text{VBF+VH}}/\mu_{\text{ggF+ttH}} = 0.7^{+2.4}_{-1.0}$ (1 VBF candidate)

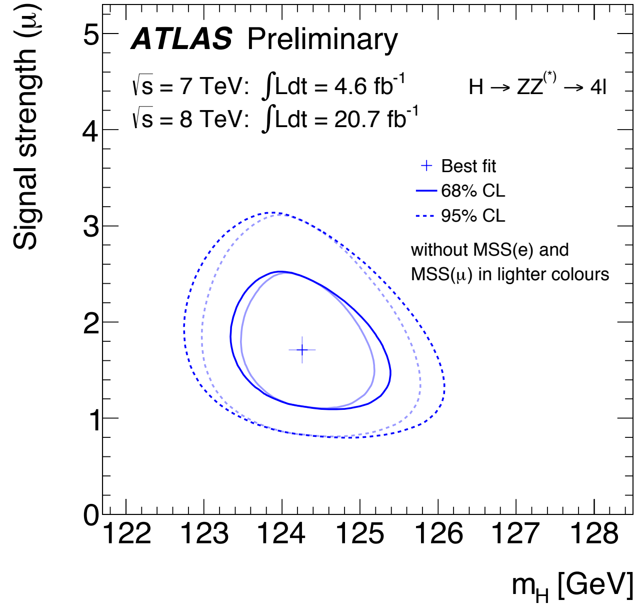

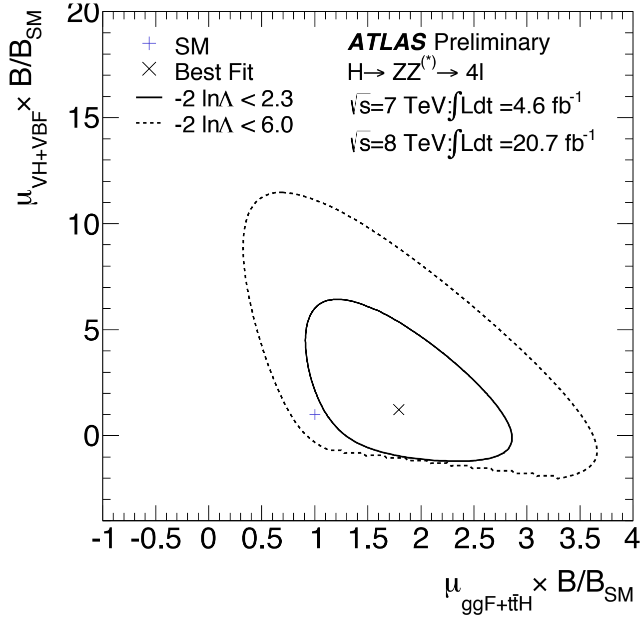

$H \rightarrow WW^{(*)} \rightarrow l\nu l\nu$ ($l=e,\mu$)

ATLAS-CONF-2013-030

1. 2 OS isolated leptons (p_T>25,15 GeV) and high E_T^{miss}
2. Categorization based on lepton flavour ($e\mu+\mu e$ or $ee+\mu\mu$) and jet multiplicity (0,1, ≥2)
3. Very different background composition for each category
4. Main backgrounds (WW, top, Z/W+j) normalized in control data, others (ZZ, WZ, $W\gamma$) from MC

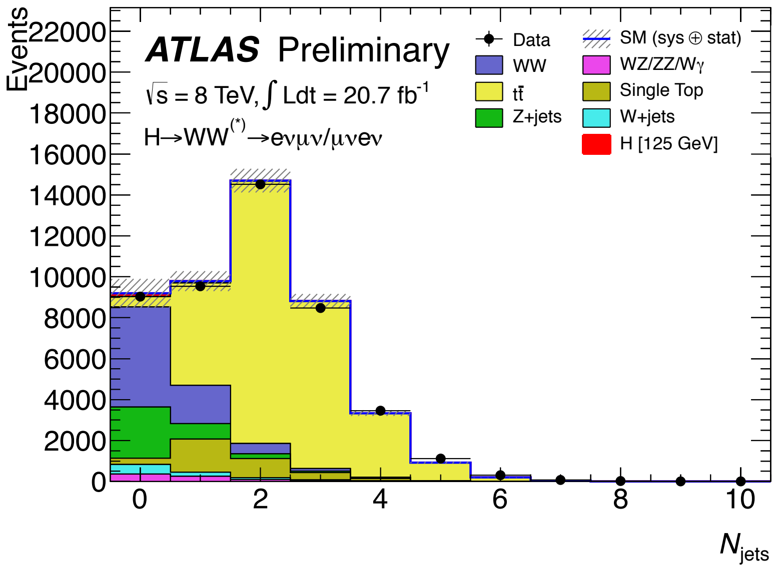

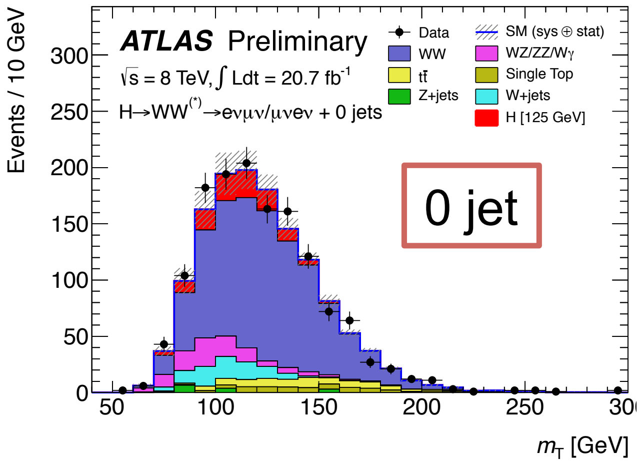

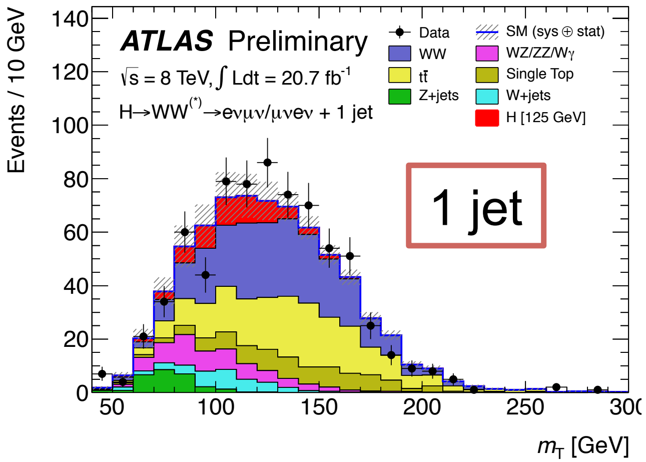

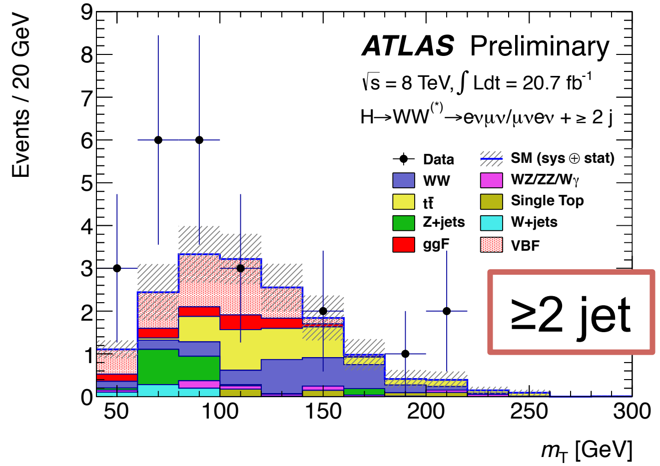

$H \to WW^{(*)} \to l\nu l\nu$: Signal strength

ATLAS-CONF-2013-030

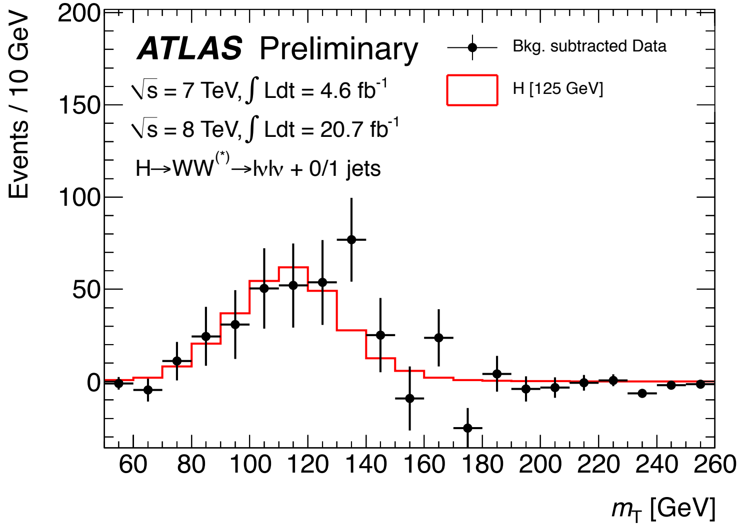

1. Observed significance at 125 GeV: 3.8σ
2. Signal strength at 125 GeV: 1.01±0.31
   [±0.21(stat)±0.19(theory)±0.12(exp.syst)±0.04(lumi)]
3. Observed significance for VBF signal at 125 GeV: 2.5σ
4. μ_{VBF} = 1.66±0.79 (ggF signal as background in the ≥2jet category and μ_{ggF} constrained in ≤1jet category)
5. μ_{ggF} = 0.82±0.36 (VBF signal as background in the ≤1jet category and μ_{VBF} constrained in ≥2jet category)

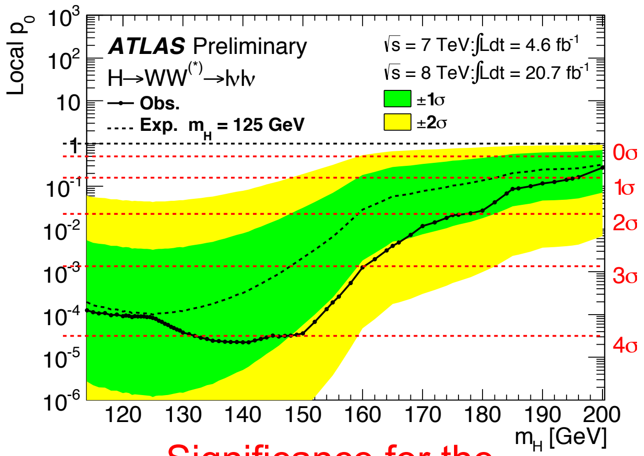

Significance for the m_H=125GeV signal

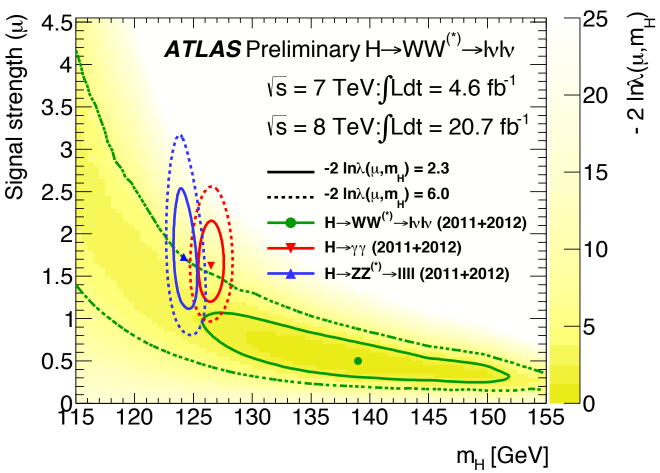

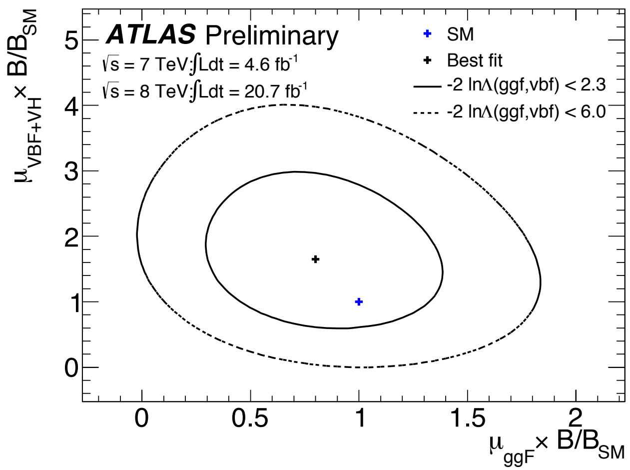

Other SM Higgs searches

13fb⁻¹@8TeV

H→ττ

1.9(1.2)×SM @125 GeV

[ATLAS-CONF-2012-160]

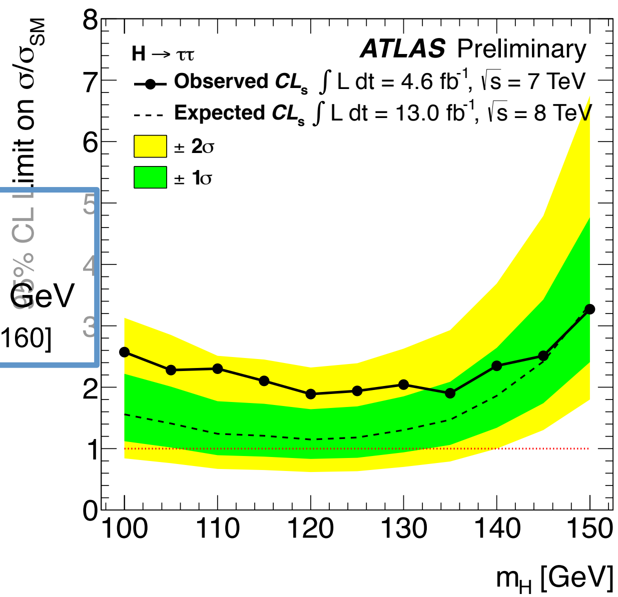

13fb⁻¹@8TeV

(W/Z)H→bb

1.8(1.9)×SM @125 GeV

[ATLAS-CONF-2012-161]

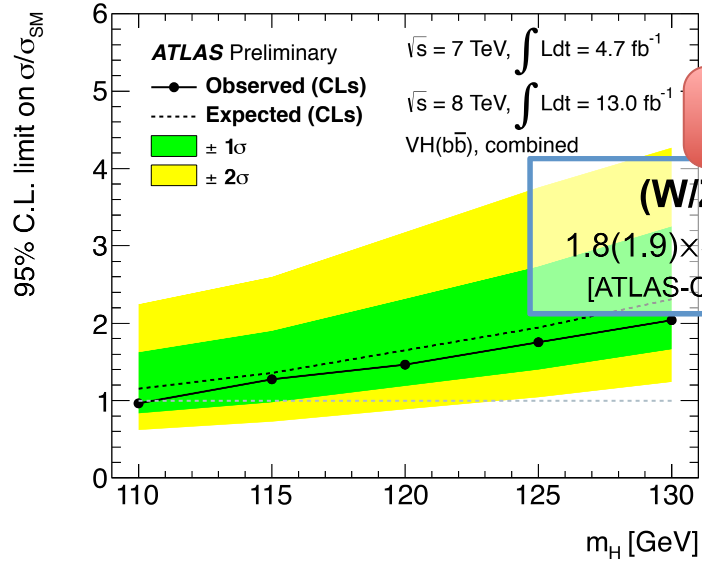

Loop-induced H→Zγ

13.5(18.2)×SM @125 GeV

[ATLAS-CONF-2013-009]

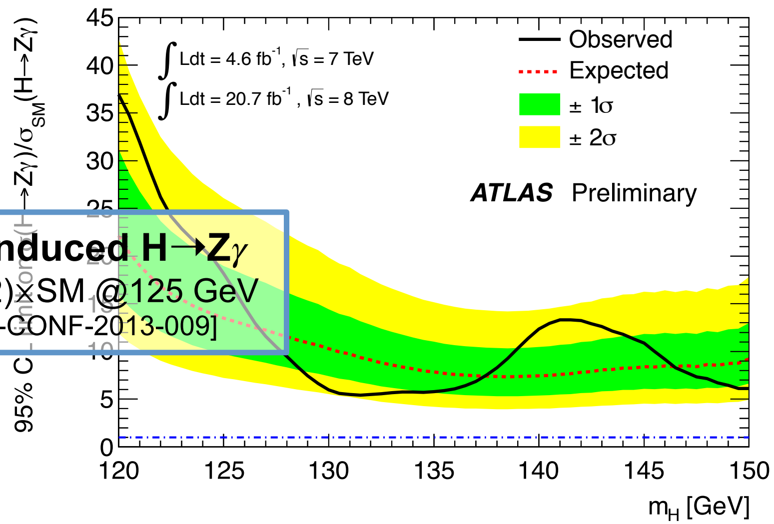

H→μμ

9.8(8.2)×SM @125 GeV

[ATLAS-CONF-2013-010]

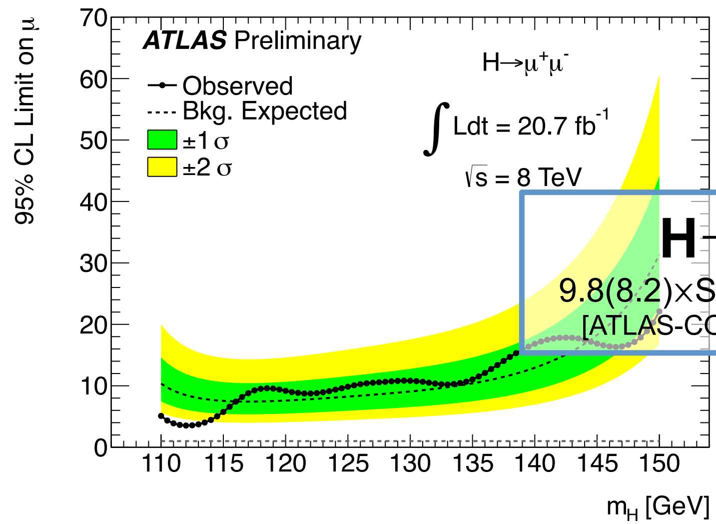

SM Higgs combination

ATLAS-CONF-2013-034

Higgs Boson Decay	Subsequent Decay	Sub-Channels	$\int L\,dt$ [fb^{-1}]	Ref.
		2011 $\sqrt{s}$ =7 TeV		
$H \to ZZ^{(*)}$	4ℓ	$\{4e, 2e2\mu, 2\mu2e, 4\mu$, 2-jet VBF, ℓ-tag$\}$	4.6	[8]
$H \to \gamma\gamma$	–	10 categories $\{p_{\mathrm{Tt}} \otimes \eta_\gamma \otimes \text{conversion}\} \oplus \{\text{2-jet VBF}\}$	4.8	[7]
$H \to WW^{(*)}$	$\ell\nu\ell\nu$	$\{ee, e\mu, \mu e, \mu\mu\} \otimes \{$0-jet, 1-jet, 2-jet VBF$\}$	4.6	[9]
$H \to \tau\tau$	$\tau_{\mathrm{lep}}\tau_{\mathrm{lep}}$	$\{e\mu\} \otimes \{$0-jet$\} \oplus \{\ell\ell\} \otimes \{$1-jet, 2-jet, $p_{\mathrm{T},\tau\tau} > 100$ GeV, $VH\}$	4.6	[10]
	$\tau_{\mathrm{lep}}\tau_{\mathrm{had}}$	$\{e, \mu\} \otimes \{$0-jet, 1-jet, $p_{\mathrm{T},\tau\tau} > 100$ GeV, 2-jet$\}$	4.6	
	$\tau_{\mathrm{had}}\tau_{\mathrm{had}}$	$\{$1-jet, 2-jet$\}$	4.6	
$VH \to Vbb$	$Z \to \nu\nu$	$E_{\mathrm{T}}^{\mathrm{miss}} \in \{120-160, 160-200, \geq 200$ GeV$\} \otimes \{$2-jet, 3-jet$\}$	4.6	[11]
	$W \to \ell\nu$	$p_{\mathrm{T}}^{W} \in \{< 50, 50-100, 100-150, 150-200, \geq 200$ GeV$\}$	4.7	
	$Z \to \ell\ell$	$p_{\mathrm{T}}^{Z} \in \{< 50, 50-100, 100-150, 150-200, \geq 200$ GeV$\}$	4.7	
		2012 $\sqrt{s}$ =8 TeV		
$H \to ZZ^{(*)}$	4ℓ	$\{4e, 2e2\mu, 2\mu2e, 4\mu$, 2-jet VBF, ℓ-tag$\}\}$	20.7	[8]
$H \to \gamma\gamma$	–	14 categories $\{p_{\mathrm{Tt}} \otimes \eta_\gamma \otimes \text{conversion}\} \oplus \{\text{2-jet VBF}\} \oplus \{\ell\text{-tag}, E_{\mathrm{T}}^{\mathrm{miss}}\text{-tag}, \text{2-jet VH}\}$	20.7	[7]
$H \to WW^{(*)}$	$\ell\nu\ell\nu$	$\{ee, e\mu, \mu e, \mu\mu\} \otimes \{$0-jet, 1-jet, 2-jet VBF$\}$	20.7	[9]
$H \to \tau\tau$	$\tau_{\mathrm{lep}}\tau_{\mathrm{lep}}$	$\{\ell\ell\} \otimes \{$1-jet, 2-jet, $p_{\mathrm{T},\tau\tau} > 100$ GeV, $VH\}$	13	[10]
	$\tau_{\mathrm{lep}}\tau_{\mathrm{had}}$	$\{e, \mu\} \otimes \{$0-jet, 1-jet, $p_{\mathrm{T},\tau\tau} > 100$ GeV, 2-jet$\}$	13	
	$\tau_{\mathrm{had}}\tau_{\mathrm{had}}$	$\{$1-jet, 2-jet$\}$	13	
$VH \to Vbb$	$Z \to \nu\nu$	$E_{\mathrm{T}}^{\mathrm{miss}} \in \{120-160, 160-200, \geq 200$ GeV$\} \otimes \{$2-jet, 3-jet$\}$	13	[11]
	$W \to \ell\nu$	$p_{\mathrm{T}}^{W} \in \{< 50, 50-100, 100-150, 150-200, \geq 200$ GeV$\}$	13	
	$Z \to \ell\ell$	$p_{\mathrm{T}}^{Z} \in \{< 50, 50-100, 100-150, 150-200, \geq 200$ GeV$\}$	13	

Mass measurement

ATLAS-CONF-2013-014, ATLAS-CONF-2013-034

High resolution channels:

1. $H \rightarrow ZZ^* \rightarrow 4l$:

- $m_H = 124.3^{+0.6}_{-0.5}(stat)\,^{+0.5}_{-0.3}(syst)$ GeV
- $4\mu(4e)$-event momentum resolution ±0.2%(0.4%),

2. $H \rightarrow \gamma\gamma$:

- $m_H = 126.8 \pm 0.2(stat) \pm 0.7(syst)$ GeV
- ±0.7GeV = energy scale uncertainty from extrapolation of photon response (0.3%), material modelling (0.3%), presampler ES (0.1%), additional syst (0.32%)

Combination: $125.5 \pm 0.2(stat)^{+0.5}_{-0.6}(syst)$ GeV

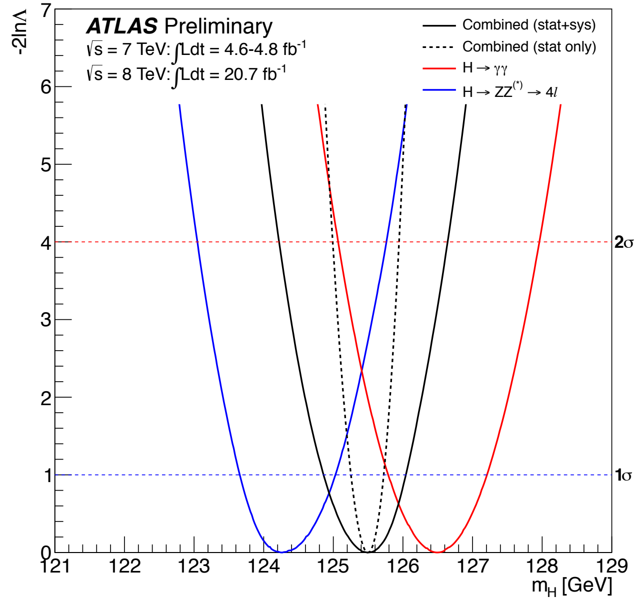

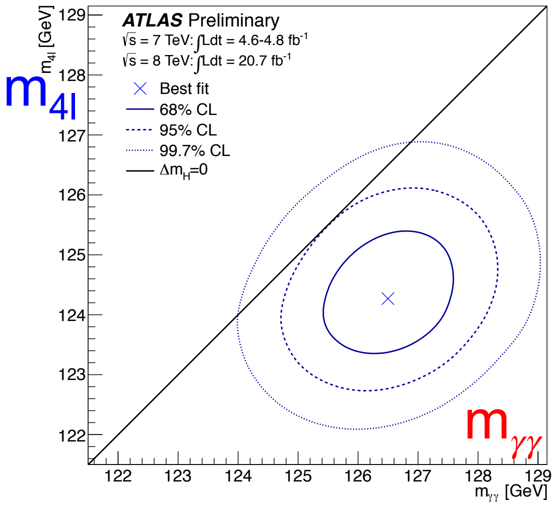

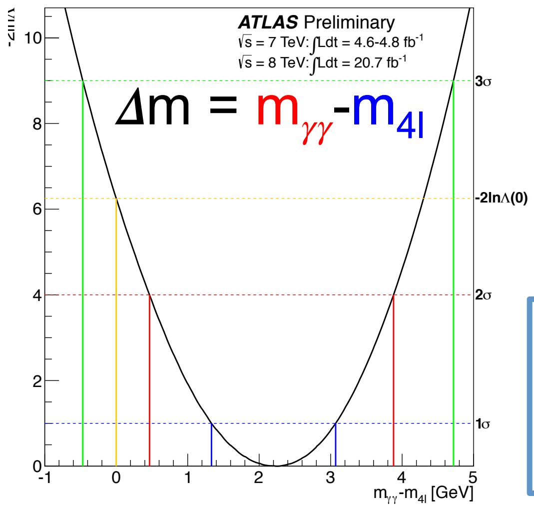

Consistency of $m_{\gamma\gamma}$ and m_{4l}:

1. correlation of e/γ energy scale
2. mass difference in m_{4e} and $m_{4\mu}$ pulls EM-scale down by 0.3% → $m_{\gamma\gamma}$ is 0.4 GeV lower

$\Delta m = 2.3^{+0.6}_{-0.7}(stat) \pm 0.6(syst)$ GeV
2.4σ (p=1.5%) from Δm=0
(p=8% with rectangular pdf's)

Signal Strengths

ATLAS-CONF-2013-034

Signal strength for individual channels

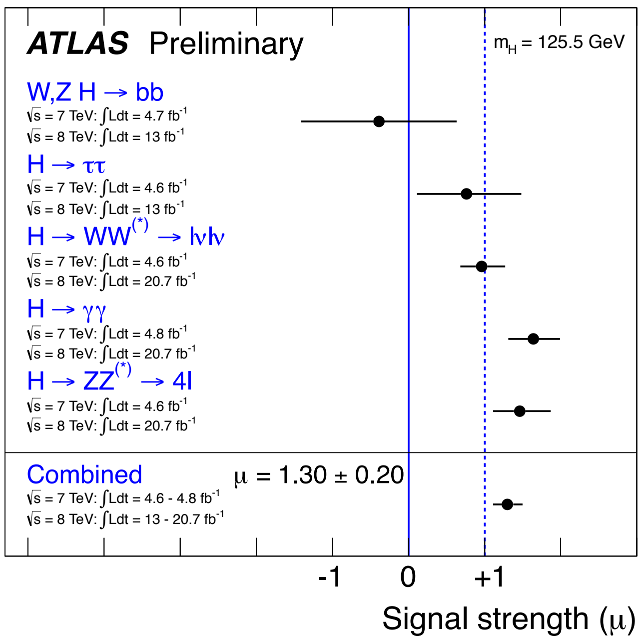

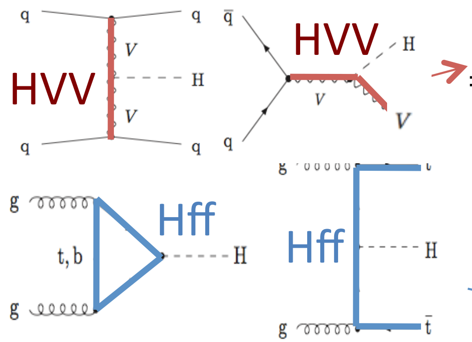

Signal strength for production modes

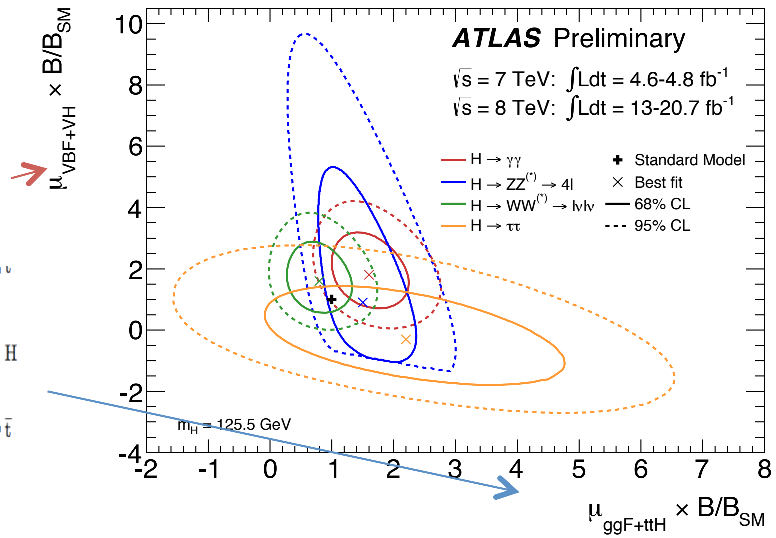

μ = *1.30±0.13(stat)±0.14(syst)*

9% compatibility with SM

(using rectangular pdf's for dominant theory systematic uncertainties, p≈40%)

Weak dependence on assumed Higgs mass

$\mu_{VBF+VH}/\mu_{ggF+ttH} = 1.2^{+0.7}_{-0.5}$

Compatible with SM expectation of unity

3.3σ from $\mu_{VBF+VH}/\mu_{ggF+ttH}$=0 hypothesis

3.1σ from $\mu_{VBF}/\mu_{ggF+ttH}$=0 hypothesis

LO Fermion vs Vector Coupling

ATLAS-CONF-2013-034

Assumptions:

- Signals observed in different channels originate from **single narrow** resonance with **m_H=125.5 GeV**
- Zero-width approximation: σxBR(ii→H→ff) = $\sigma_{ii} \cdot \Gamma_{ff} / \Gamma_H$
- Tensor structure of the couplings assumed to be SM, only coupling strengths are modified with scale factors k

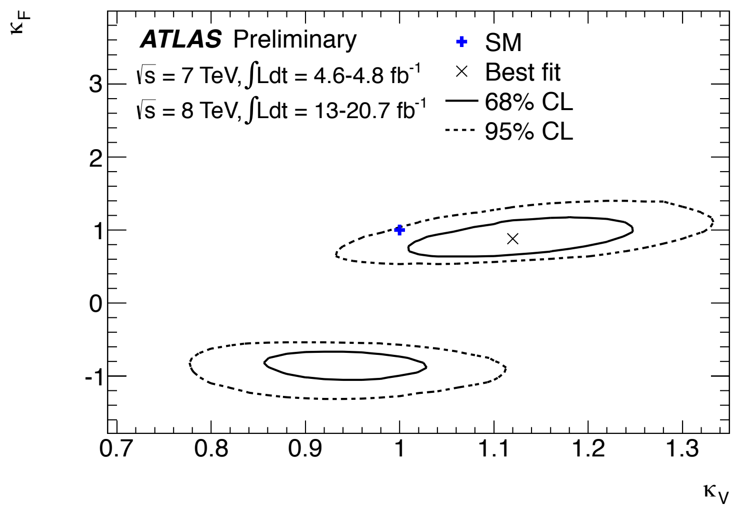

1. Consistent treatment of tree-level couplings in Higgs production and decay
2. Vector coupling scale factor $k_V = k_W = k_Z$
3. Fermion coupling scale factor $k_F = k_t = k_b = k_\tau = k_g$
4. Only SM contributions in H→$\gamma\gamma$ and gg→H loops and in Higgs decays
5. Sensitivity to relative sign from interference in H→$\gamma\gamma$ loop
6. 8% compatibility with SM hypothesis
7. Vector coupling k_V directly and indirectly constrained
8. Fermion coupling k_F still not directly constrained, but only indirectly from ggF-dominated channels

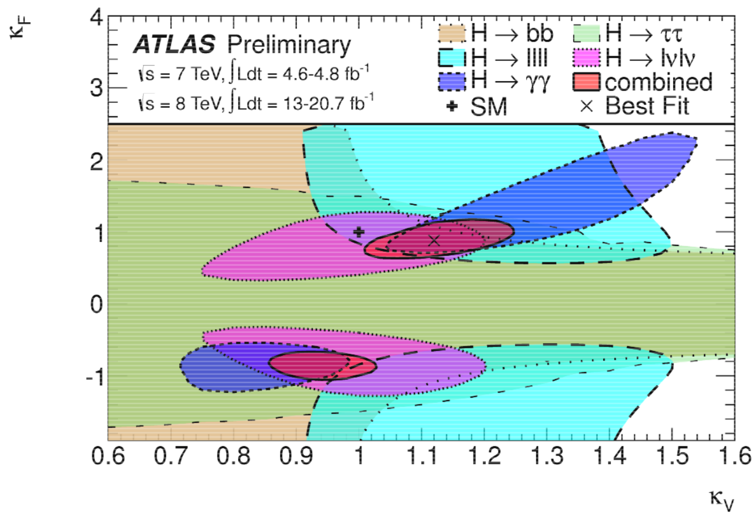

Coupling Fits

ATLAS-CONF-2013-034

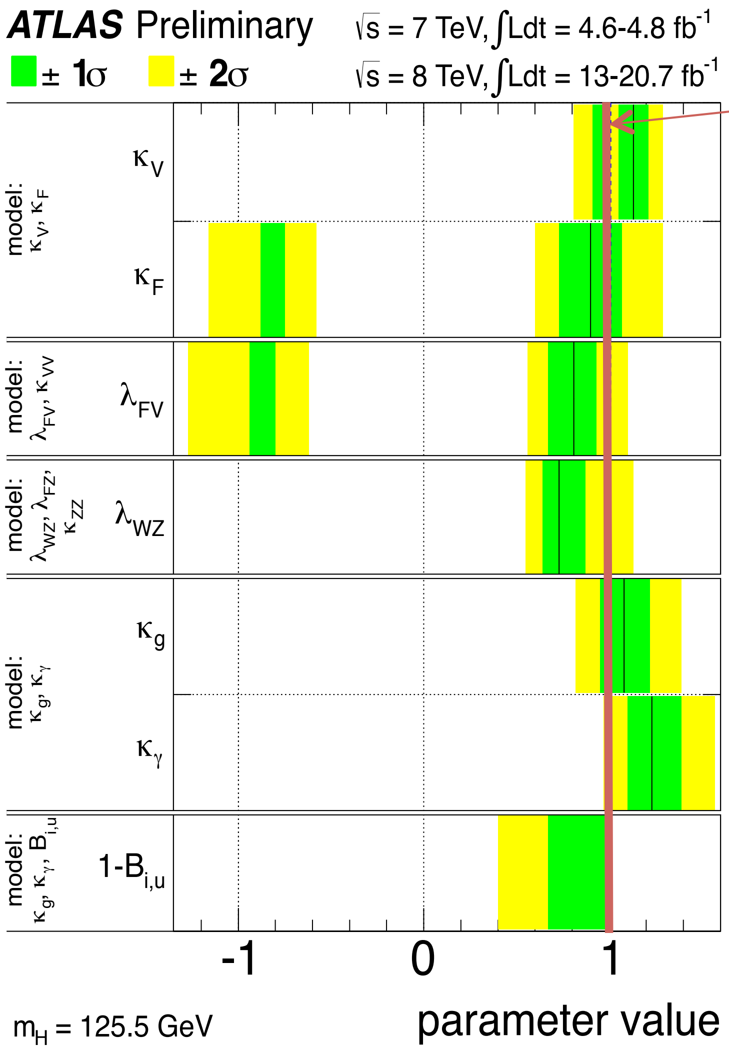

SM Expectation

- Fermion vs Vector couplings (only SM contributions to total width)
- Fermion vs Vector couplings (no assumption on total width)
- Custodial symmetry of W and Z couplings
- BSM effects in ggF and $H \rightarrow \gamma\gamma$ loops (only SM contributions to total width, other k=1)
- BSM effects in loops and decay (no assumption on total width, other k=1)

Spin-parity

$H \to \gamma\gamma$

ATLAS-CONF-2013-012

1. Spin-1 hypothesis disfavoured by Landau-Yang theorem
2. Comparison of the SM 0^+ hypothesis with the 2^+_m "graviton-like" with minimal couplings (produced via gg and qqbar)
3. Discriminating variable: polar angle θ^* in the resonance rest frame
4. Analysis performed with a 2D fit of $m_{\gamma\gamma}$ and $\cos\theta^*$

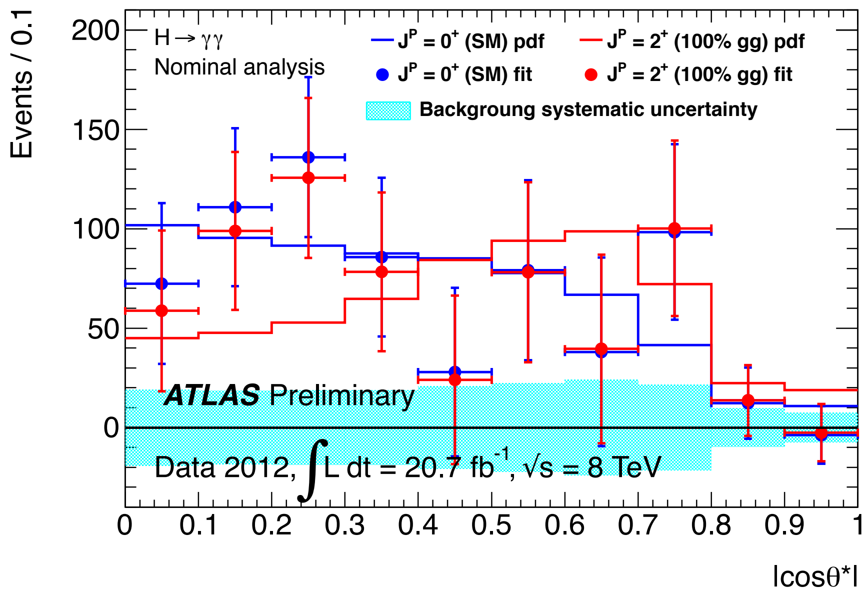

Slightly different data points because of the subtraction of the profiled background in the SM and spin-2 fits

- Data in good agreement with the 0^+ hypothesis
- 2^+ resonance produced via gluon fusion excluded at 99% CL
- Lower sensitivity in case of mixture of gg and qqbar production modes for the 2^+ model

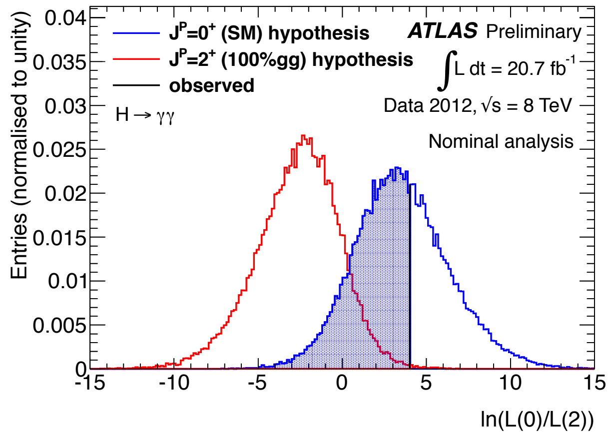

H→ZZ(*)→4l

ATLAS-CONF-2013-013

1. Discriminants (BDT and MELA) combining kinematics of production and decay (5 angles and 2 Z masses)
2. SM 0^+ hypothesis tested vs 0^-, $1^{\pm}$,$2^{\pm}$
3. 43 events in $115<m_{4l}<130$ used

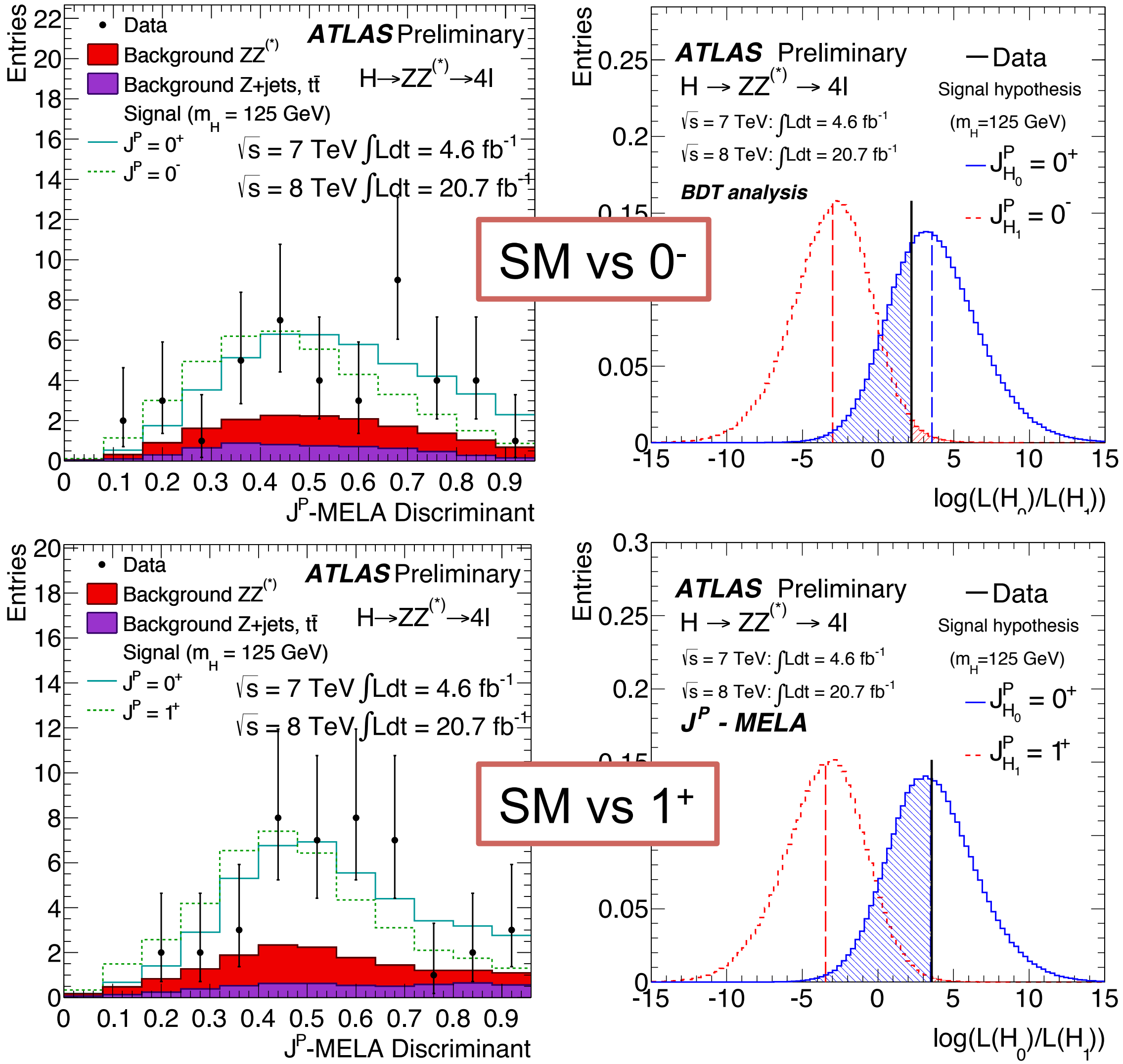

- Observed p_0 favours SM against 0^-,1^+,1^-,2^+ and 2^-
- 0^- and 1^+ excluded at >97.8% CL

$H \to WW^{(*)} \to l\nu l\nu$

ATLAS-CONF-2013-031

1. Only $e\nu\mu\nu$ events with 0 jets in 8TeV data used here with slightly different event selection
2. SM 0^+ hypothesis vs 2^+_m
3. Discriminating variables: m_{ll}, $\Delta\phi_{ll}$, p_T^{ll} and m_T
4. 2D fit of the output of 2 BDTs, each trained for one spin hypothesis (BDT_0 and BDT_2)

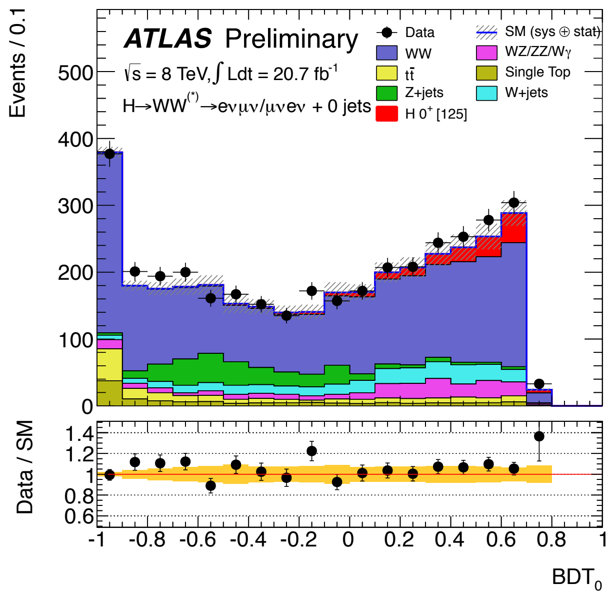

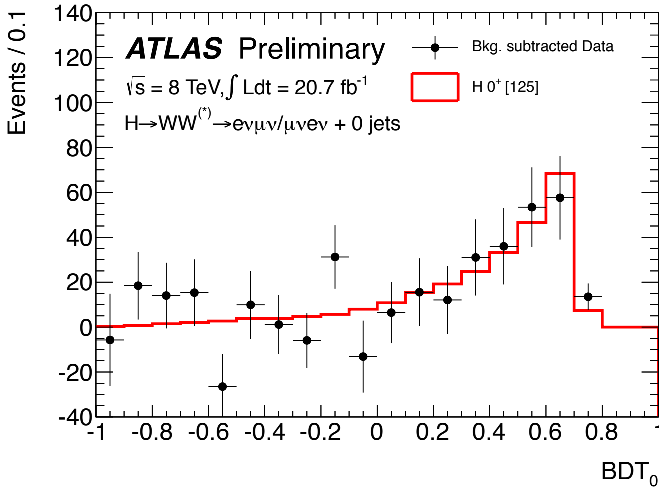

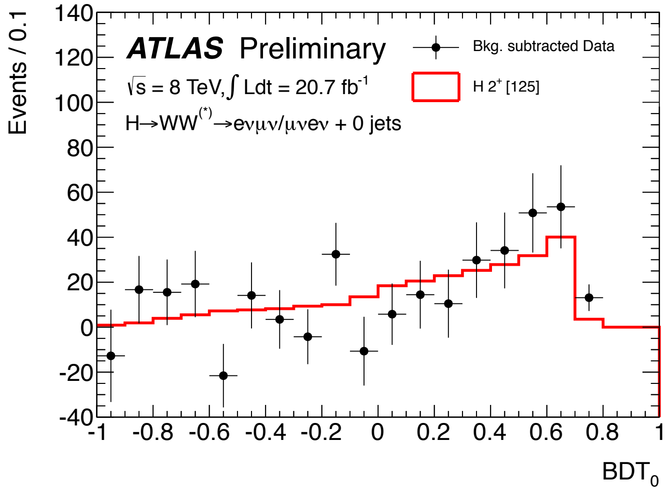

2^+_m hypothesis excluded at 95-99% CL_S depending on the production mode (gg or qqbar)

Slightly different data points because of the subtraction of the profiled background in the SM and spin-2 fits

Spin Combination

ATLAS-CONF-2013-040

1. Combination of spin studies in $H\rightarrow\gamma\gamma$, $H\rightarrow ZZ^*\rightarrow 4l$ and $H\rightarrow WW^*\rightarrow e\nu\mu\nu$
2. SM 0^+ hypothesis and 2^+_m "graviton-like" with minimal coupling to SM particles
3. Test with different fractions of gg and qq, f_{qq}, productions
4. Agreement with SM hypothesis in all individuals channels
5. Channels complementary in sensitivity for low/high f_{qq}

2^+_m hypothesis excluded for any production admixture at more than 99.9% CL_S

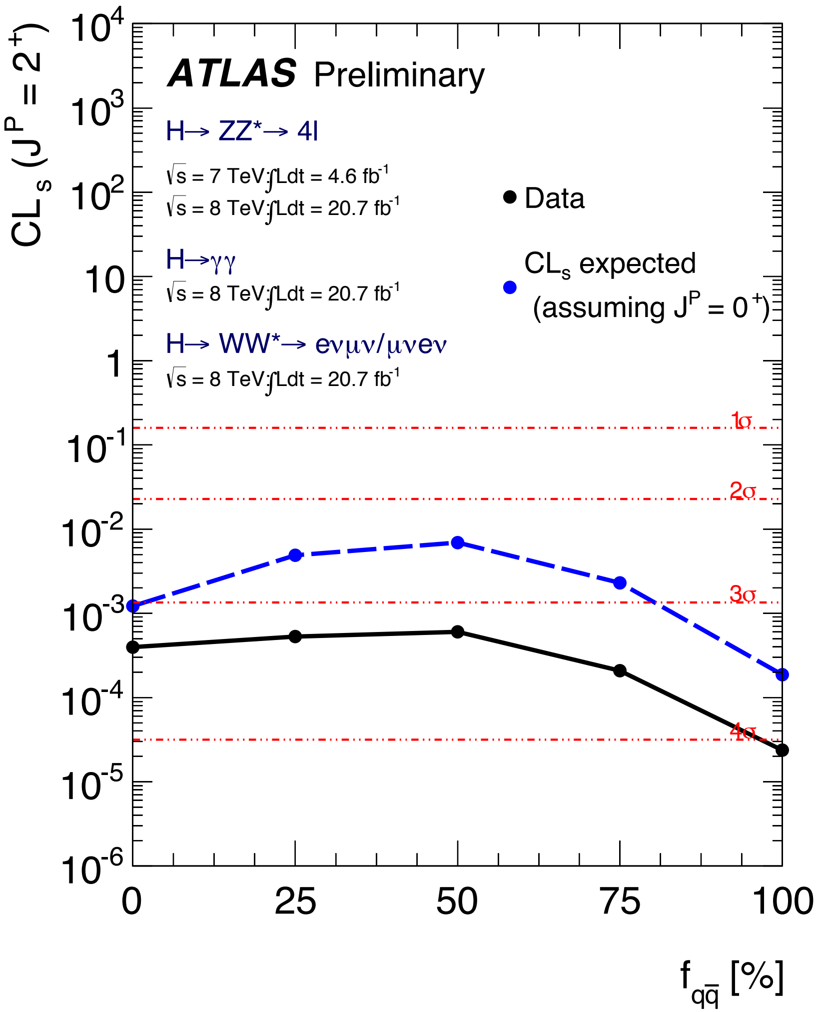

Summary

1. Preliminary results based on full 2012 datasets in $H \to \gamma\gamma$, $H \to ZZ^* \to 4l$ and $H \to WW^* \to l\nu l\nu$
2. Independent observations in all three channels: a lot of Higgs candidates to be used for property measurements!
3. $m_H = 125.5 \pm 0.2(\text{stat})^{+0.5}_{-0.6}(\text{syst})$ GeV
4. $\mu = 1.30 \pm 0.13(\text{stat}) \pm 0.14(\text{syst})$
5. $\mu_{VBF+VH}/\mu_{ggF+ttH} = 1.2^{+0.7}_{-0.5}$
6. 3.1σ evidence of VBF production
7. Higgs couplings consistent with SM within 2σ
8. SM 0^+ hypothesis preferred against 0^-, $1^\pm$ and $2^\pm$
9. 2^+_m "graviton-like" particle excluded at ≥99.9% CL_S

So far no significant deviation from SM, more stringent measurements expected with the updated results in the fermionic decays

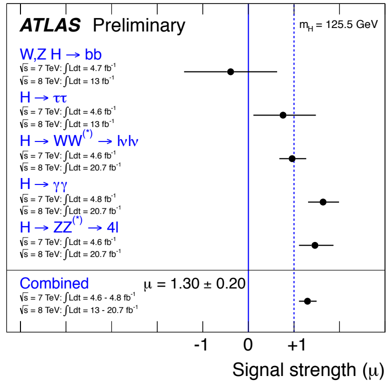

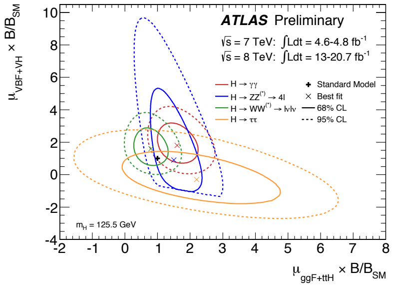

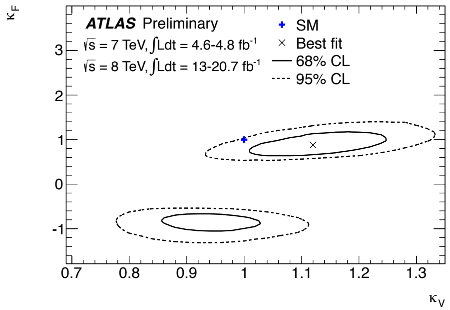

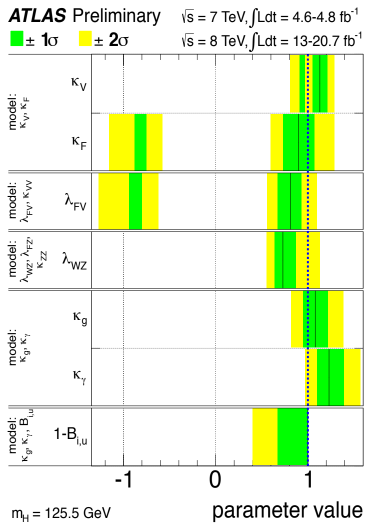

Backup Slides

ATLAS

Max-Planck-Institut für Physik
(Werner-Heisenberg-Institut)

ATLAS Detector

L ~ 46 m, Ø ~ 22 m, 7000 tons
~10^8 electronic channels

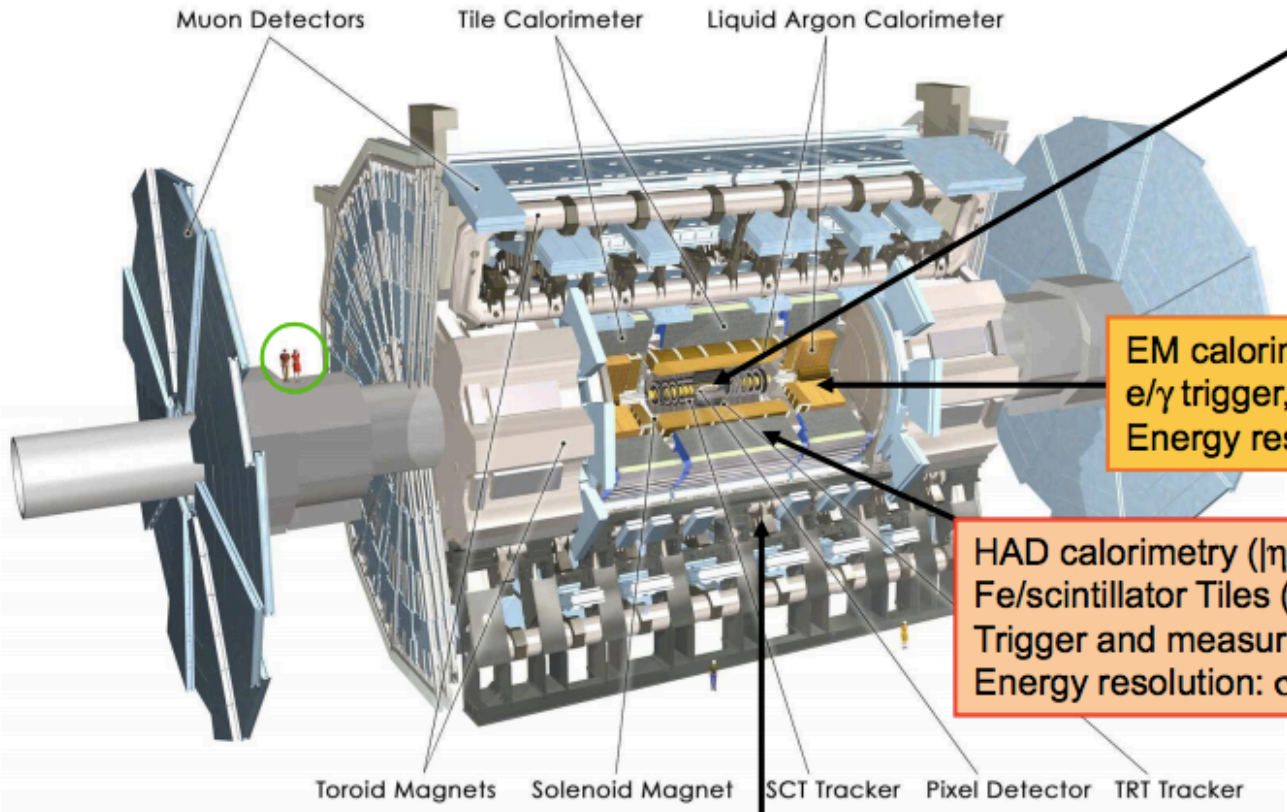

Inner Tracker ($|\eta|<2.5$, B=2T):
Si Pixels, Si strips, Transition Radiation detector (straws).
Precise tracking and vertexing, e/π separation.
Momentum resolution:
$\sigma/p_T \sim 0.04\%\ p_T(\text{GeV}) \oplus 1.5\%$

EM calorimeter: Pb-LAr Accordion.
e/γ trigger, identification and measurement
Energy resolution: $\sigma/E \sim 10\%/\sqrt{E} \oplus 0.7\%$

HAD calorimetry ($|\eta|<5$): segmentation, hermeticity.
Fe/scintillator Tiles (central), Cu/W-LAr (forward).
Trigger and measurement of jets and missing E_T.
Energy resolution: $\sigma/E \sim 50\%/\sqrt{E} \oplus 3\%$

3-level trigger reducing the rate from 40 MHz to ~200 Hz

Muon Spectrometer ($|\eta|<2.7$) : air-core toroids with gas-based muon chambers.
Muon trigger and measurement with momentum resolution < 10% up to $E_\mu \sim 1$ TeV

From F.Hubaut's slide at MoriondEW 2013

$m^2_{\gamma\gamma} = 2E_{\gamma 1}E_{\gamma 2}(1-\cos\theta)$

ATLAS-CONF-2012-091, ATLAS-CONF-2012-168, , ATLAS-CONF-2013-012

Fraction of γ candidates per conversion status

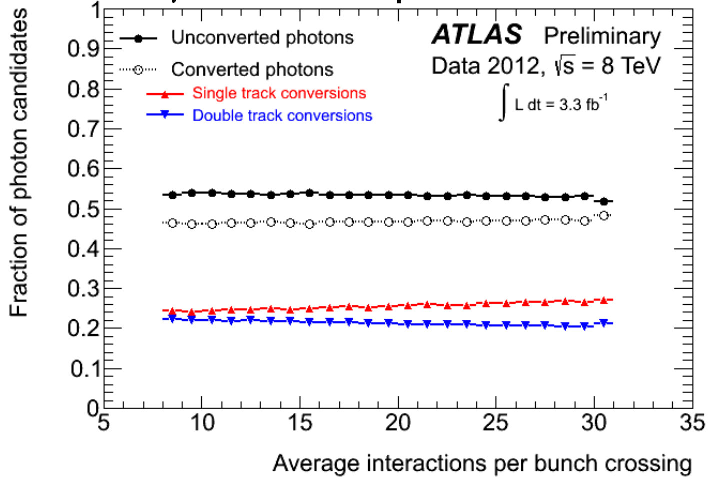

Stability of EM calo response vs pileup

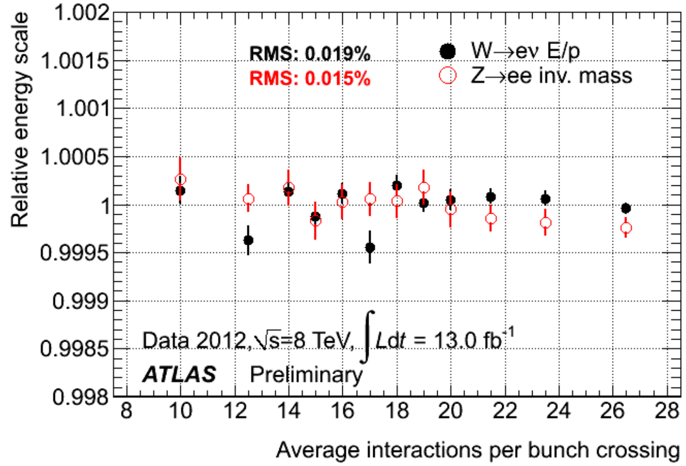

Efficiency to select the primary vertex

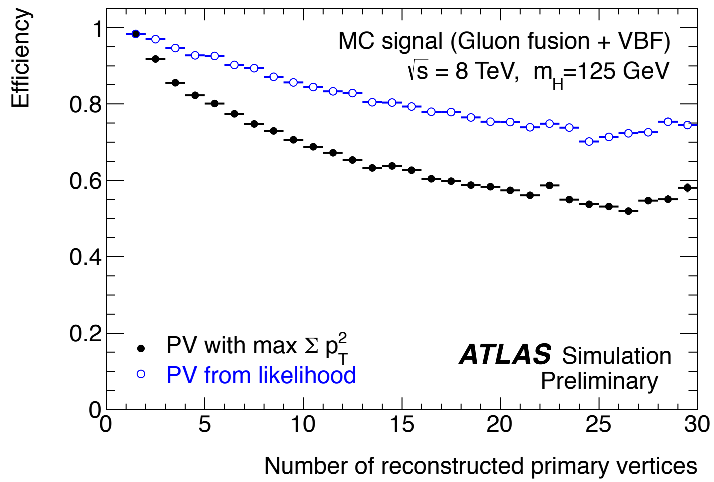

Mass resolution vs pileup

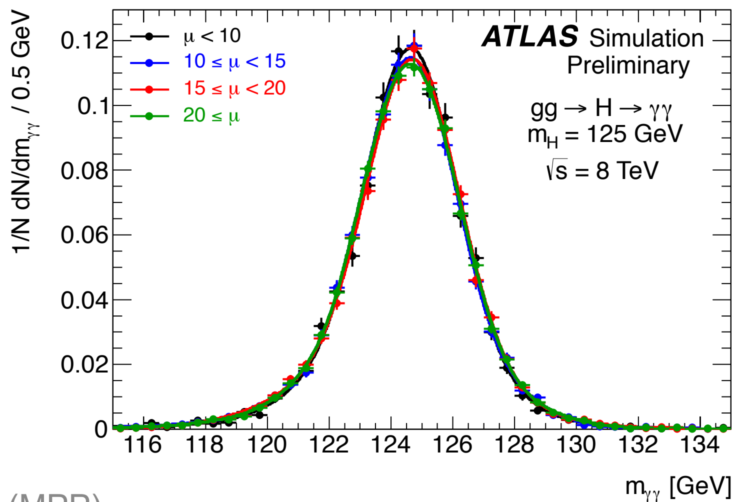

H→γγ: Categories

ATLAS-CONF-2012-091, ATLAS-CONF-2012-168, , ATLAS-CONF-2013-012

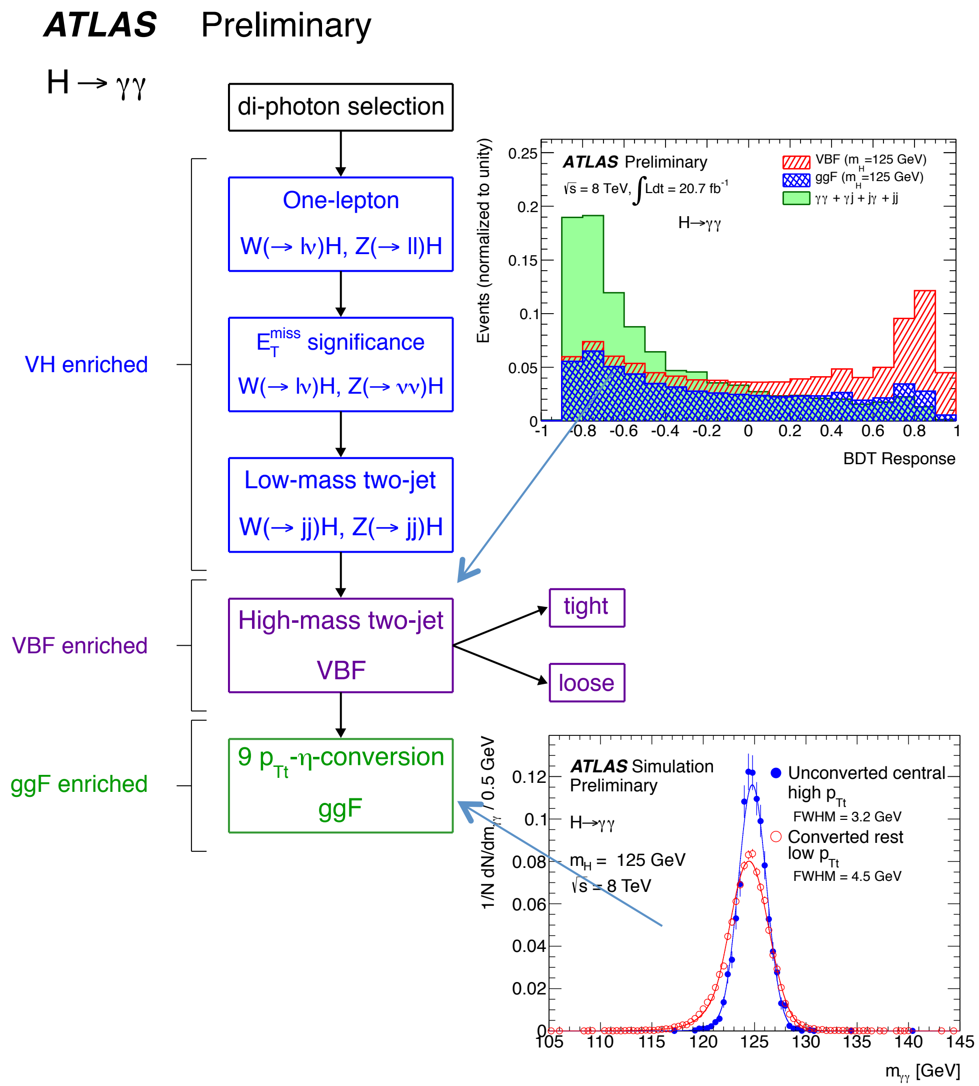

Category	Parametrisation	Uncertainty [N_{evt}] $\sqrt{s}$ = 7 TeV	Uncertainty [N_{evt}] $\sqrt{s}$ = 8 TeV
Inclusive	4th order pol.	7.3	12.0
Unconverted central, low p_{Tt}	Exp. of 2nd order pol.	2.1	4.6
Unconverted central, high p_{Tt}	Exponential	0.2	0.8
Unconverted rest, low p_{Tt}	4th order pol.	2.2	11.4
Unconverted rest, high p_{Tt}	Exponential	0.5	2.0
Converted central, low p_{Tt}	Exp. of 2nd order pol.	1.6	2.4
Converted central, high p_{Tt}	Exponential	0.3	0.8
Converted rest, low p_{Tt}	4th order pol.	4.6	8.0
Converted rest, high p_{Tt}	Exponential	0.5	1.1
Converted transition	Exp. of 2nd order pol.	3.2	9.1
Loose high-mass two-jet	Exponential	0.4	1.1
Tight high-mass two-jet	Exponential	-	0.3
Low-mass two-jet	Exponential	-	0.6
E_T^{miss} significance	Exponential	-	0.1
One-lepton	Exponential	-	0.3

$\sqrt{s}$	8 TeV						
Category	N_D	N_S	$gg \to H$ [%]	VBF [%]	WH [%]	ZH [%]	ttH [%]
Unconv. central, low p_{Tt}	10900	51.8	93.7	4.0	1.4	0.8	0.2
Unconv. central, high p_{Tt}	553	7.9	79.3	12.6	4.1	2.5	1.4
Unconv. rest, low p_{Tt}	41236	107.9	93.2	4.0	1.6	1.0	0.1
Unconv. rest, high p_{Tt}	2558	16.0	78.1	13.3	4.7	2.8	1.1
Conv. central, low p_{Tt}	7109	33.1	93.6	4.0	1.3	0.9	0.2
Conv. central, high p_{Tt}	363	5.1	78.9	12.6	4.3	2.7	1.5
Conv. rest, low p_{Tt}	38156	97.8	93.2	4.1	1.6	1.0	0.1
Conv. rest, high p_{Tt}	2360	14.4	77.7	13.0	5.2	3.0	1.1
Conv. transition	14864	40.1	90.7	5.5	2.2	1.3	0.2
Loose high-mass two-jet	276	5.3	45.0	54.1	0.5	0.3	0.1
Tight high-mass two-jet	136	8.1	23.8	76.0	0.1	0.1	0.0
Low-mass two-jet	210	3.3	48.1	3.0	29.7	17.2	1.9
E_T^{miss} significance	49	1.3	4.1	0.5	35.7	47.6	12.1
One-lepton	123	2.9	2.2	0.6	63.2	15.4	18.6
All categories (inclusive)	118893	395.0	88.0	7.3	2.7	1.5	0.5

H→$\gamma\gamma$: Systematics

ATLAS-CONF-2013-012

Syst uncert on signal yield

Table 5: Summary of the im[...] for the analysis of the 8 TeV data.

Systematic uncertainties	Value(%)	Constraint
Luminosity	±3.6	
Trigger	±0.5	
Photon Identification	±2.4	Log-normal
Isolation	±1.0	
Photon Energy Scale	±0.25	
Branching ratio	±5.9% – ±2.1% (m_H = 110 - 150 GeV)	Asymmetric Log-normal
Scale	ggF: $^{+7.2}_{-7.8}$ VBF: $^{+0.2}_{-0.2}$ WH: $^{+0.2}_{-0.6}$ ZH: $^{+1.6}_{-1.5}$ ttH: $^{+3.8}_{-9.3}$	Asymmetric Log-normal
PDF+α_s	ggF: $^{+7.5}_{-6.9}$ VBF: $^{+2.6}_{-2.7}$ WH: ±3.5 ZH: ±3.6 ttH: ±7.8	Asymmetric Log-normal
Theory cross section on ggF	Tight high-mass two-jet: ±48 Loose high-mass two-jet: ±28 Low-mass two-jet: ±30	Log-normal

Syst uncert on category migrations

Table 6: [...]sis of the 8 TeV data.

Systematic uncertainties	Category	Value(%)			Constraint
Underlying Event	Tight high-mass two-jet	ggF: ±8.8	VBF: ±2.0	VH, ttH: ±8.8	Log-normal
	Loose high-mass two-jet	ggF: ±12.8	VBF: ±3.3	VH, ttH: ±12.8	
	Low-mass two-jet	ggF: ±12	VBF: ±3.9	VH, ttH: ±12	
Jet Energy Scale	Low p_{Tt}	ggF: −0.1	VBF: −1.0	Others: −0.1	Gaussian
	High p_{Tt}	ggF: −0.7	VBF: −1.3	Others: +0.4	
	Tight high-mass two-jet	ggF: +11.8	VBF: +6.7	Others: +20.2	
	Loose high-mass two-jet	ggF: +10.7	VBF: +4.0	Others: +5.7	
	Low-mass two-jet	ggF: +4.7	VBF: +2.6	Others: 1.4	
	E_T^{miss}significance	ggF: 0.0	VBF: 0.0	Others: 0.0	
	one-lepton	ggF: 0.0	VBF: 0.0	Others: −0.1	
Jet Energy Resolution	Low p_{Tt}	ggF: 0.0	VBF: 0.2	Others: 0.0	Gaussian
	High p_{Tt}	ggF: −0.2	VBF: 0.2	Others: 0.6	
	Tight high-mass two-jet	ggF: 3.8	VBF: −1.3	Others: 7.0	
	Loose high-mass two-jet	ggF: 3.4	VBF: −0.7	Others: 1.2	
	Low-mass two-jet	ggF: 0.5	VBF: 3.4	Others: −1.3	
	E_T^{miss}significance	ggF: 0.0	VBF: 0.0	Others: 0.0	
	one-lepton	ggF: −0.9	VBF: −0.5	Others: −0.1	
η^* modelling		Tight high-mass two-jet: +7.6 Loose high-mass two-jet: +6.2			Gaussian
Dijet angular modelling		Tight high-mass two-jet: +12.1 Loose high-mass two-jet: +8.5			Gaussian
Higgs p_T		Low p_{Tt}: +1.3 High p_{Tt}: −10.2 Tight high-mass two-jet: −10.4 Loose high-mass two-jet: −8.5 Low-mass two-jet: −12.5 E_T^{miss}significance: −2.0 one-lepton : −4.0			Gaussian
Material Mismodelling		Unconv: −4.0	Conv: +3.5		Gaussian
JVF	Loose High-mass two-jet	ggF: −1.2	VBF: −0.3	Others: −1.2	Gaussian
	Low-mass two-jet	ggF: −2.3	VBF: −2.4	Others: −2.3	
E_T^{miss}	E_T^{miss}significance	ggF: +66.4	VBF: +30.7	VH, ttH: +1.2	Gaussian
e reco and identification		one-lepton: < 1			Gaussian
e Escale and resolution		one-lepton: < 1			Gaussian
μ reco, ID resolution		one-lepton: < 1			Gaussian
μ spectrometer resolution		one-lepton: 0			Gaussian

1. Signal mass resolution dominated by extrap from electron to photon response (14-23%)
2. Mass uncertainties (0.55%):
   1. extrap of photon response (0.3%)
   2. material modelling (0.3%)
   3. presampler ES (0.1%)
   4. additional syst (0.32%)

$H \rightarrow ZZ^{(*)} \rightarrow 4l$

ATLAS-CONF-2013-013

Latest improvements:
- tighter electron ID
- mass measurement with constrained fit to Z mass
- lepton pairing
- looser requirement on the second Z
- inclusion of FSR for muons
- Categorization in ggF/VBF/VH

method	estimate at $\sqrt{s}$ = 8 TeV	estimate at $\sqrt{s}$ = 7 TeV
	4μ	4μ
m_{12} fit: Z + jets contribution	$2.4 \pm 0.5 \pm 0.6^\dagger$	$0.22 \pm 0.07 \pm 0.02^\dagger$
m_{12} fit: $t\bar{t}$ contribution	$0.14 \pm 0.03 \pm 0.03^\dagger$	$0.03 \pm 0.01 \pm 0.01^\dagger$
$t\bar{t}$ from $e\mu + \mu\mu$	$0.10 \pm 0.05 \pm 0.004$	-
	$2e2\mu$	$2e2\mu$
m_{12} fit: Z + jets contribution	$2.5 \pm 0.5 \pm 0.6^\dagger$	$0.19 \pm 0.06 \pm 0.02^\dagger$
m_{12} fit: $t\bar{t}$ contribution	$0.10 \pm 0.02 \pm 0.02^\dagger$	$0.03 \pm 0.01 \pm 0.01^\dagger$
$t\bar{t}$ from $e\mu + \mu\mu$	$0.12 \pm 0.07 \pm 0.005$	-
	$2\mu 2e$	$2\mu 2e$
$\ell\ell + e^\pm e^\mp$ relaxed cuts	$5.2 \pm 0.4 \pm 0.5^\dagger$	$1.8 \pm 0.3 \pm 0.4$
$\ell\ell + e^\pm e^\mp$ inverted cuts	$3.9 \pm 0.4 \pm 0.6$	-
$3\ell + \ell$ (same-sign)	$4.3 \pm 0.6 \pm 0.5$	$2.8 \pm 0.4 \pm 0.5^\dagger$
sub-leading same sign full analysis events	4	0
	$4e$	$4e$
$\ell\ell + e^\pm e^\mp$ relaxed cuts	$3.2 \pm 0.5 \pm 0.4^\dagger$	$1.4 \pm 0.3 \pm 0.4$
$\ell\ell + e^\pm e^\mp$ inverted cuts	$3.6 \pm 0.6 \pm 0.6$	-
$3\ell + \ell$ (same-sign)	$4.2 \pm 0.5 \pm 0.5$	$2.5 \pm 0.3 \pm 0.5^\dagger$
sub-leading same sign full analysis events	3	2

Reducible background (tt,Z+jets) normalized in control regions:
- ll+**μμ** (tt,Zbb), no isolation cut and fail impact parameter cut
- ll+**ee** Bkg (mis-ID'ed hadrons, photon conversion, heavy flavor decay), relaxing ID on sub-leading electrons

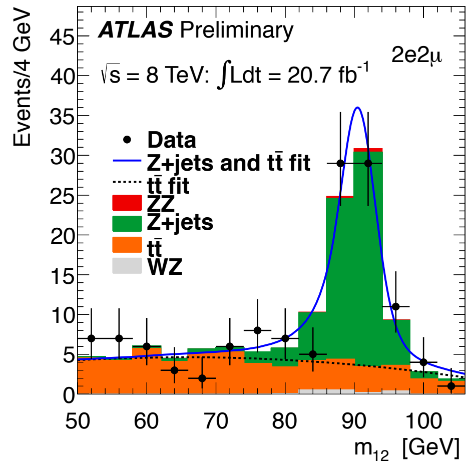

Control regions with no iso and IP cuts on sub-leading pair:

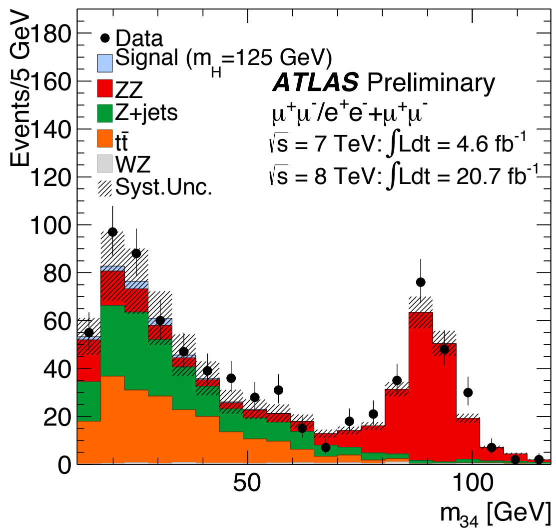

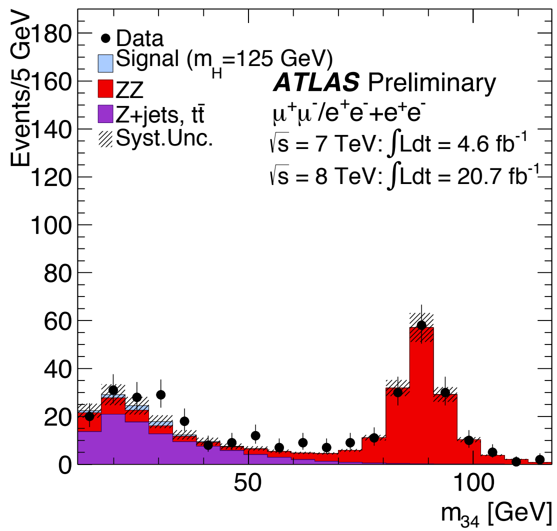

H→ZZ(*)→4l: Mass Resolution

ATLAS-CONF-2013-013

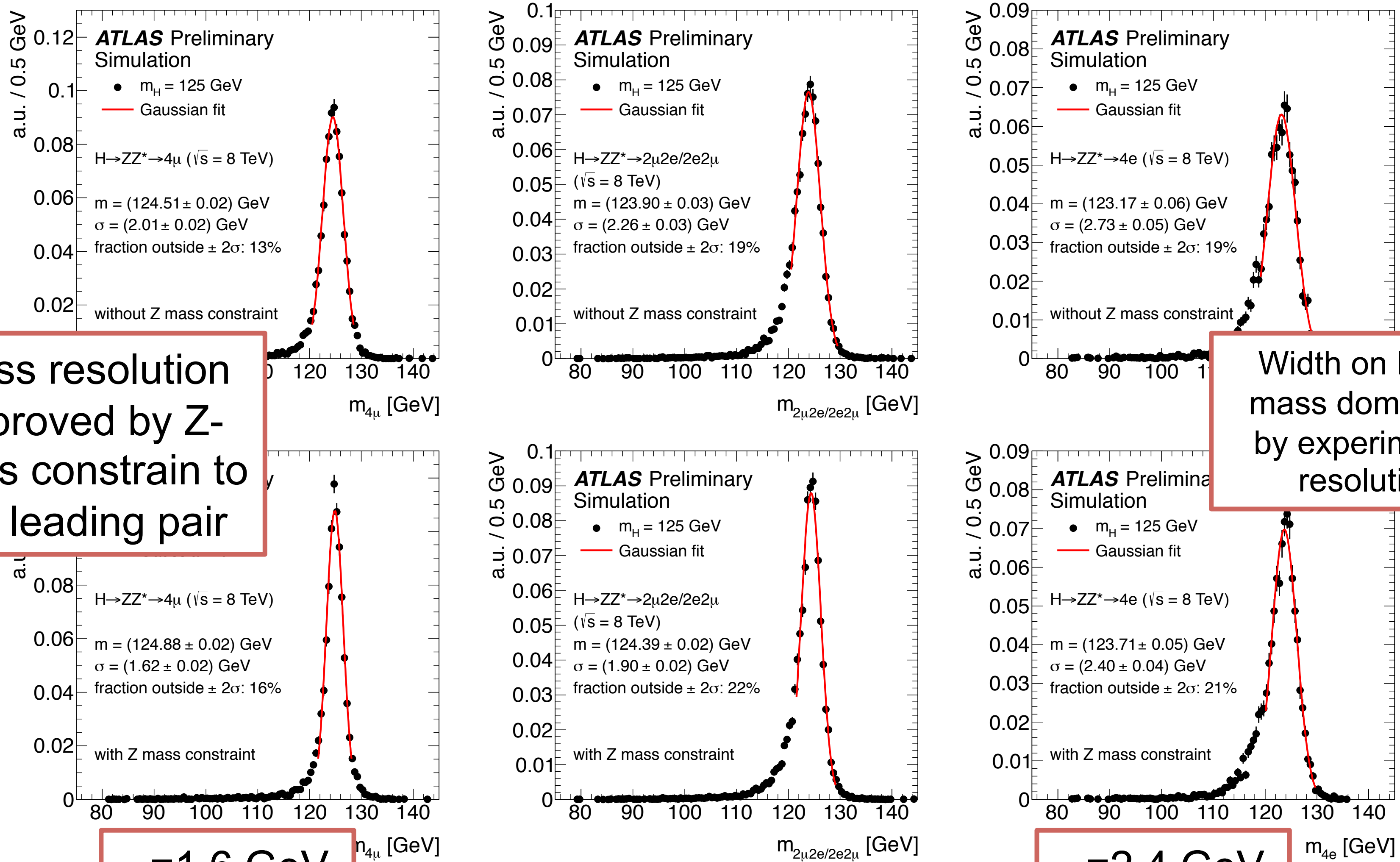

Mass resolution improved by Z-mass constrain to the leading pair

Width on Higgs mass dominated by experimental resolution

σ=1.6 GeV

σ=2.4 GeV

$H \to ZZ^{(*)} \to 4l$: Systematics

ATLAS-CONF-2013-013

Systematics on measurement of signal mass		
	Electron energy scale	Muon energy scale
4μ	-	±0.2%
$2\mu 2e$	-	±0.1%
$2e2\mu$	±0.2%	-
4e	±0.4%	-

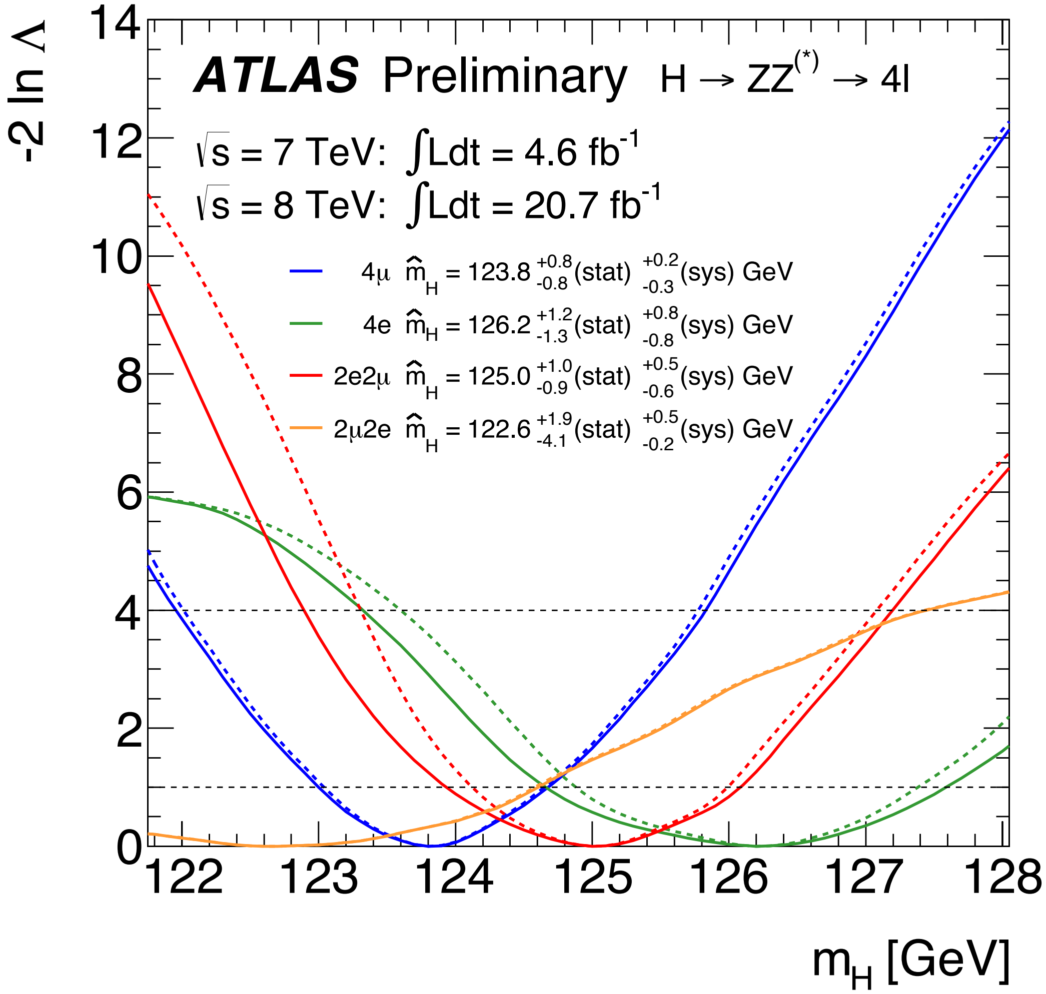

$H \rightarrow ZZ^{(*)} \rightarrow 4l$

ATLAS-CONF-2013-013

Table 7: The numbers of expected signal events for the m_H=125 GeV hypothesis and background events together with the numbers of observed events, in a window of ±5 GeV around 125 GeV for 20.7 fb^{-1} at $\sqrt{s}$ = 8 TeV and 4.6 fb^{-1} at $\sqrt{s}$ = 7 TeV as well as for their combination.

	total signal full mass range	signal	$ZZ^{(*)}$	$Z+\text{jets}, t\bar{t}$	S/B	expected	observed
			$\sqrt{s}$ = 8 TeV				
4μ	5.8 ± 0.7	5.3 ± 0.7	2.3 ± 0.1	0.50 ± 0.13	1.9	8.1 ± 0.9	11
$2\mu 2e$	3.0 ± 0.4	2.6 ± 0.4	1.2 ± 0.1	1.01 ± 0.21	1.2	4.8 ± 0.7	4
$2e2\mu$	4.0 ± 0.5	3.4 ± 0.4	1.7 ± 0.1	0.51 ± 0.16	1.5	5.6 ± 0.7	6
$4e$	2.9 ± 0.4	2.3 ± 0.3	1.0 ± 0.1	0.62 ± 0.16	1.4	3.9 ± 0.6	6
total	15.7 ± 2.0	13.7 ± 1.8	6.2 ± 0.4	2.62 ± 0.34	1.6	22.5 ± 2.9	27
			$\sqrt{s}$ = 7 TeV				
4μ	1.0 ± 0.1	0.97 ± 0.13	0.49 ± 0.02	0.05 ± 0.02	1.8	1.5 ± 0.2	2
$2\mu 2e$	0.4 ± 0.1	0.39 ± 0.05	0.21 ± 0.02	0.55 ± 0.12	0.5	1.2 ± 0.1	1
$2e2\mu$	0.7 ± 0.1	0.57 ± 0.08	0.33 ± 0.02	0.04 ± 0.01	1.5	0.9 ± 0.1	2
$4e$	0.4 ± 0.1	0.29 ± 0.04	0.15 ± 0.01	0.49 ± 0.12	0.5	0.9 ± 0.1	0
total	2.5 ± 0.4	2.2 ± 0.3	1.17 ± 0.07	1.12 ± 0.17	1.0	4.5 ± 0.5	5
			$\sqrt{s}$ = 8 TeV and $\sqrt{s}$ = 7 TeV				
4μ	6.8 ± 0.8	6.3 ± 0.8	2.8 ± 0.1	0.55 ± 0.15	1.9	9.6 ± 1.0	13
$2\mu 2e$	3.4 ± 0.5	3.0 ± 0.4	1.4 ± 0.1	1.56 ± 0.33	1.0	6.0 ± 0.8	5
$2e2\mu$	4.7 ± 0.6	4.0 ± 0.5	2.1 ± 0.1	0.55 ± 0.17	1.5	6.6 ± 0.8	8
$4e$	3.3 ± 0.5	2.6 ± 0.4	1.2 ± 0.1	1.11 ± 0.28	1.1	4.9 ± 0.8	6
total	18.2 ± 2.4	15.9 ± 2.1	7.4 ± 0.4	3.74 ± 0.93	1.4	27.1 ± 3.4	32

$H \rightarrow ZZ^{(*)} \rightarrow 4l$

ATLAS-CONF-2013-013

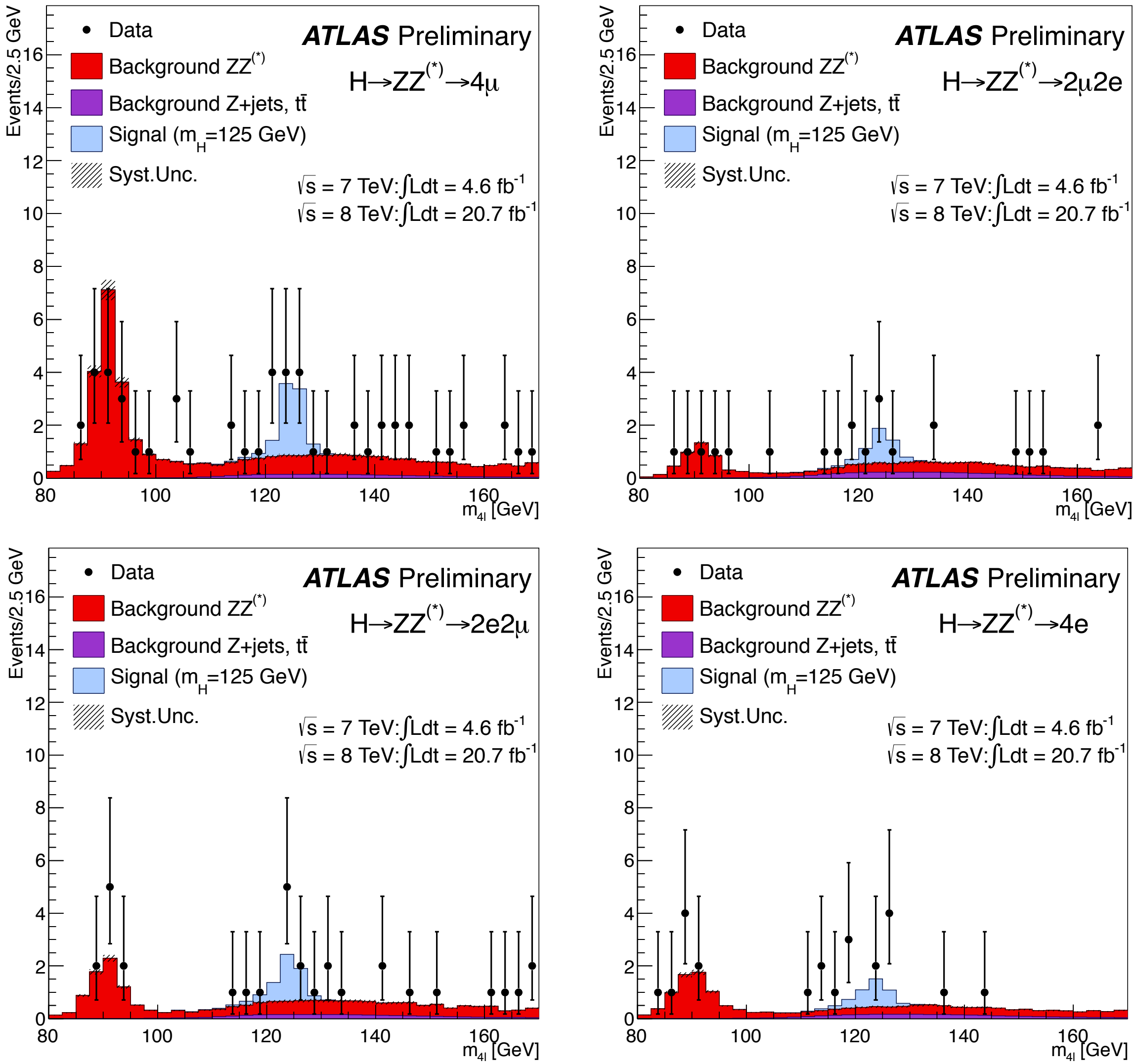

H→ZZ(*)→4l

ATLAS-CONF-2013-013

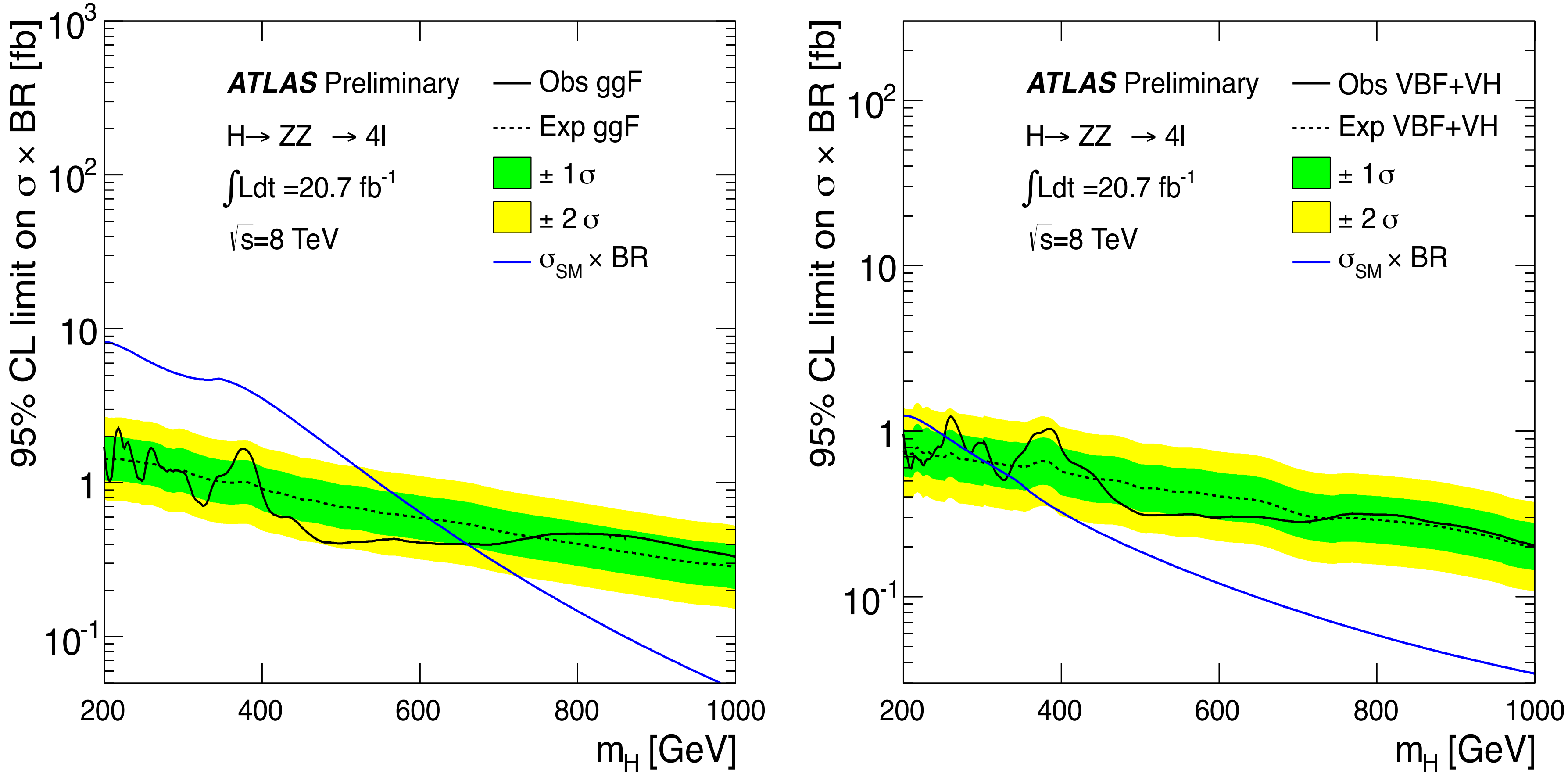

$H \rightarrow ZZ^{(*)} \rightarrow 4l$

ATLAS-CONF-2013-013

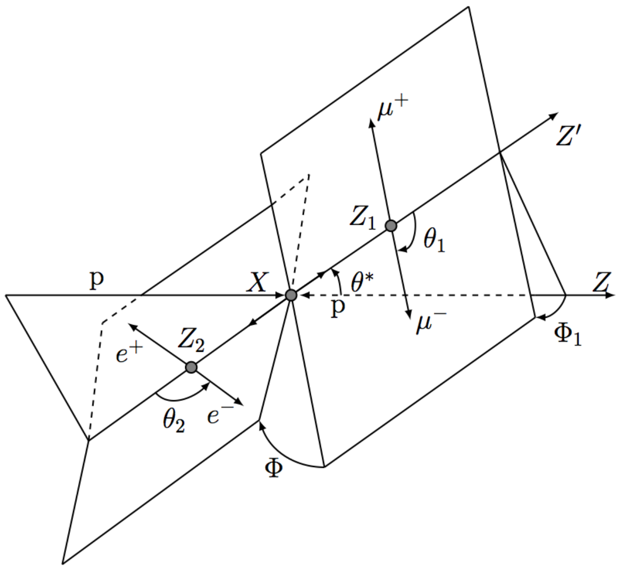

Table 9: For an assumed 0^+ hypothesis H_0, the values for the expected and observed p_0-values of the different tested spin and parity hypotheses H_1 for the BDT and J^P-MELA analyses. The results are given combining the $\sqrt{s}$ = 8 TeV and $\sqrt{s}$ = 7 TeVdata sets. Also given is the observed p_0-value where 0^+ is the test hypothesis and the other spins states are the assumed hypothesis (observed*). These two observed p_0-values are combined to provide the CL_S confidence level for each test hypothesis. The production mode is assumed to be 100% ggF.

		BDT analysis				J^P-MELA analysis			
		tested J^P for an assumed 0^+		tested 0^+ for an assumed J^P	CL_S	tested J^P for an assumed 0^+		tested 0^+ for an assumed J^P	CL_S
		expected	observed	observed*		expected	observed	observed*	
0^-	p_0	0.0037	0.015	0.31	0.022	0.0011	0.0022	0.40	0.004
1^+	p_0	0.0016	0.001	0.55	0.002	0.0031	0.0028	0.51	0.006
1^-	p_0	0.0038	0.051	0.15	0.060	0.0010	0.027	0.11	0.031
2^+_m	p_0	0.092	0.079	0.53	0.168	0.064	0.11	0.38	0.182
2^-	p_0	0.0053	0.25	0.034	0.258	0.0032	0.11	0.08	0.116

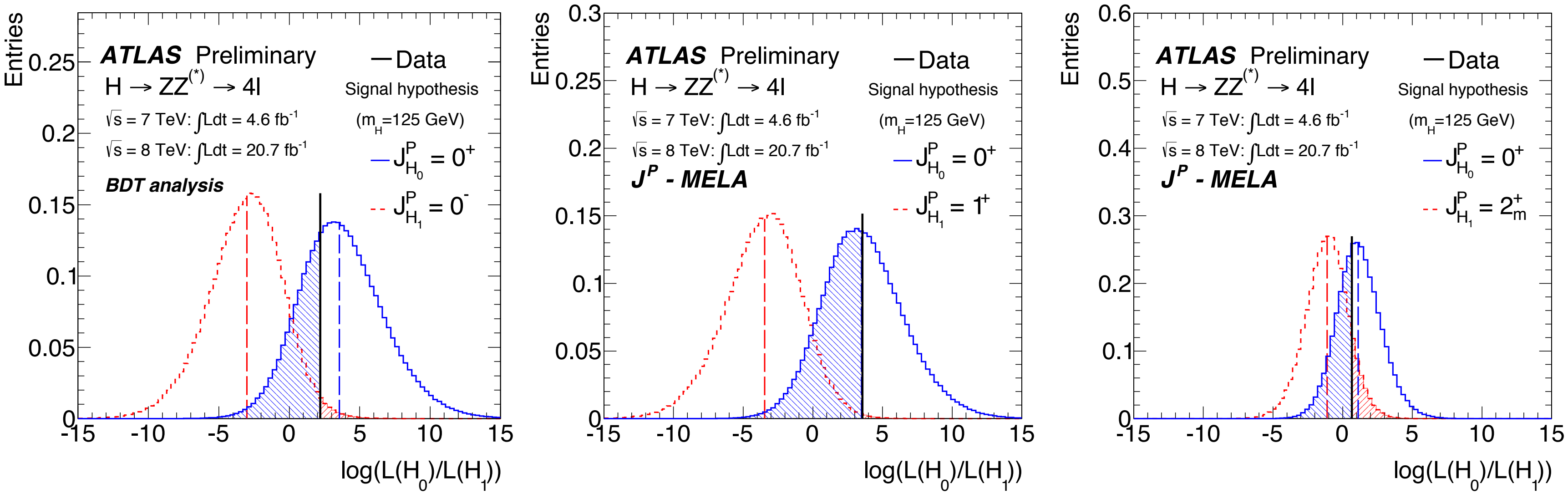

$H \rightarrow WW^{(*)} \rightarrow l\nu l\nu$ ($l=e,\mu$)

ATLAS-CONF-2013-030

Category	$N_{\rm jet}=0$	$N_{\rm jet}=1$	$N_{\rm jet}\geq 2$
Pre-selection	Two isolated leptons ($\ell=e,\mu$) with opposite charge Leptons with $p_{\rm T}^{\rm lead}>25$ and $p_{\rm T}^{\rm sublead}>15$ $e\mu+\mu e$: $m_{\ell\ell}>10$ $ee+\mu\mu$: $m_{\ell\ell}>12$, $\lvert m_{\ell\ell}-m_Z\rvert>15$		
Missing transverse momentum and hadronic recoil	$e\mu+\mu e$: $E_{\rm T,rel}^{\rm miss}>25$ $ee+\mu\mu$: $E_{\rm T,rel}^{\rm miss}>45$ $ee+\mu\mu$: $p_{\rm T,rel}^{\rm miss}>45$ $ee+\mu\mu$: $f_{\rm recoil}<0.05$	$e\mu+\mu e$: $E_{\rm T,rel}^{\rm miss}>25$ $ee+\mu\mu$: $E_{\rm T,rel}^{\rm miss}>45$ $ee+\mu\mu$: $p_{\rm T,rel}^{\rm miss}>45$ $ee+\mu\mu$: $f_{\rm recoil}<0.2$	$e\mu+\mu e$: $E_{\rm T}^{\rm miss}>20$ $ee+\mu\mu$: $E_{\rm T}^{\rm miss}>45$ $ee+\mu\mu$: $E_{\rm T,STVF}^{\rm miss}>35$ -
General selection	- $\lvert\Delta\phi_{\ell\ell,MET}\rvert>\pi/2$ $p_{\rm T}^{\ell\ell}>30$	$N_{b\text{-jet}}=0$ - $e\mu+\mu e$: $Z/\gamma^*\rightarrow\tau\tau$ veto	$N_{b\text{-jet}}=0$ $p_{\rm T}^{\rm tot}<45$ $e\mu+\mu e$: $Z/\gamma^*\rightarrow\tau\tau$ veto
VBF topology	- - - -	- - - -	$m_{jj}>500$ $\lvert\Delta y_{jj}\rvert>2.8$ No jets ($p_{\rm T}>20$) in rapidity gap Require both ℓ in rapidity gap
$H\rightarrow WW^{(*)}\rightarrow\ell\nu\ell\nu$ topology	$m_{\ell\ell}<50$ $\lvert\Delta\phi_{\ell\ell}\rvert<1.8$ $e\mu+\mu e$: split $m_{\ell\ell}$ Fit $m_{\rm T}$	$m_{\ell\ell}<50$ $\lvert\Delta\phi_{\ell\ell}\rvert<1.8$ $e\mu+\mu e$: split $m_{\ell\ell}$ Fit $m_{\rm T}$	$m_{\ell\ell}<60$ $\lvert\Delta\phi_{\ell\ell}\rvert<1.8$ - Fit $m_{\rm T}$

$H \to WW^{(*)} \to l\nu l\nu$ ($l=e,\mu$)

ATLAS-CONF-2013-030

Table 12: Leading systematic uncertainties on the expected event yields for the 8 TeV analysis. The first four rows are calculated for inclusive $N_{\rm jet}$ modes and redistributed to exclusive ones (Section 5). The QCD scale uncertainties on the inclusive ggF cross sections are anti-correlated between the exclusive $N_{\rm jet}$ modes. Some uncertainties are grouped differently with respect to Table 11 to reflect the treatment of correlations; most experimental ones are correlated between the signal and background. Sources contributing less than 4% to any column, and individual entries below 1%, are omitted.

	Signal processes (%)			Background processes (%)		
Source	$N_{\rm jet}=0$	$N_{\rm jet}=1$	$N_{\rm jet}\geq 2$	$N_{\rm jet}=0$	$N_{\rm jet}=1$	$N_{\rm jet}\geq 2$
Theoretical uncertainties						
QCD scale for ggF signal for $N_{\rm jet}\geq 0$	13	-	-	-	-	-
QCD scale for ggF signal for $N_{\rm jet}\geq 1$	10	27	-	-	-	-
QCD scale for ggF signal for $N_{\rm jet}\geq 2$	-	15	4	-	-	-
QCD scale for ggF signal for $N_{\rm jet}\geq 3$	-	-	4	-	-	-
Parton shower and UE model (signal only)	3	10	5	-	-	-
PDF model	8	7	3	1	1	1
$H\to WW$ branching ratio	4	4	4	-	-	-
QCD scale (acceptance)	4	4	3	-	-	-
WW normalisation	-	-	-	1	2	4
Experimental uncertainties						
Jet energy scale and resolution	5	2	6	2	3	7
b-tagging efficiency	-	-	-	-	7	2
$f_{\rm recoil}$ efficiency	1	1	-	4	2	-

$H \rightarrow WW^{(*)} \rightarrow l\nu l\nu$ ($l=e,\mu$)

ATLAS-CONF-2013-030

Table 13: Leading uncertainties on the signal strength μ for the combined 7 and 8 TeV analysis.

Category	Source	Uncertainty, up (%)	Uncertainty, down (%)
Statistical	Observed data	+21	–21
Theoretical	Signal yield ($\sigma \cdot \mathcal{B}$)	+12	–9
Theoretical	WW normalisation	+12	–12
Experimental	Objects and DY estimation	+9	–8
Theoretical	Signal acceptance	+9	–7
Experimental	MC statistics	+7	–7
Experimental	$W+$ jets fake factor	+5	–5
Theoretical	Backgrounds, excluding WW	+5	–4
Luminosity	Integrated luminosity	+4	–4
Total		+32	–29

$H \to WW^{(*)} \to l\nu l\nu$ ($l=e,\mu$)

ATLAS-CONF-2013-031

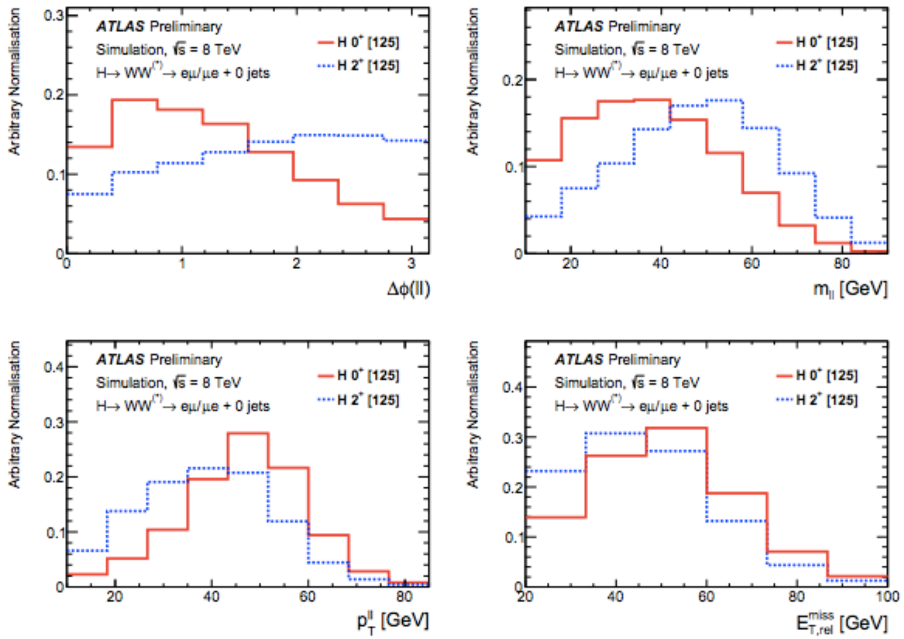

Source	Uncertainty (%)
Jet energy scale & resolution	± 9
WW normalisation, theory	± 9
W+jets fake factor	± 8
Lepton scale & resolution	± 6
Other backgrounds, theory	± 5
Pileup modelling	± 4
PDF model	± 4
E_T^{miss} scale & resolution	± 3

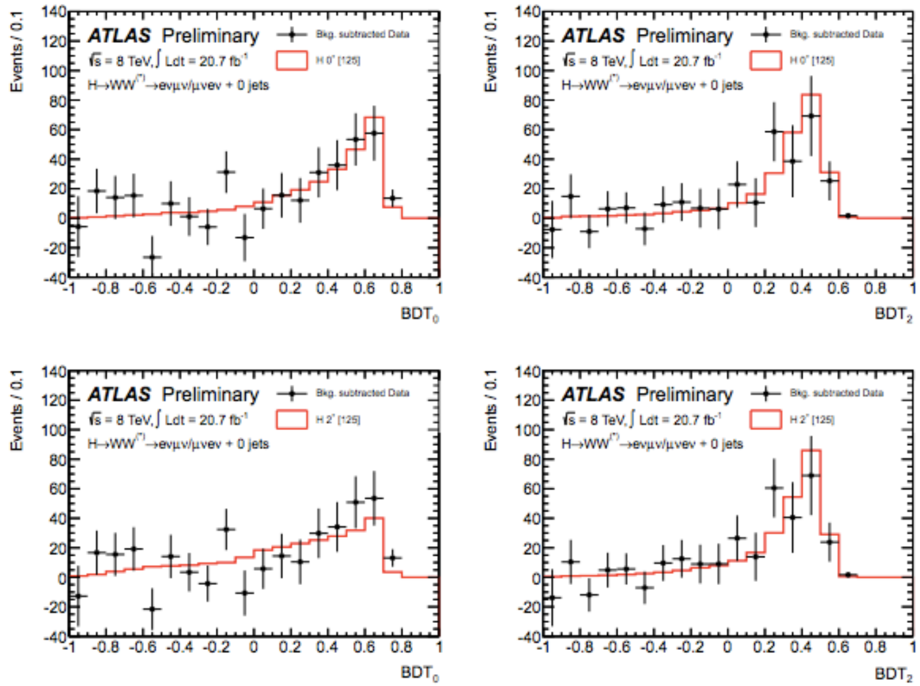

Profile Likelihood Ratio

ATLAS-CONF-2013-014

$$\Lambda(\mu) = \frac{L(\mu, \hat{\hat{\theta}}(\mu))}{L(\hat{\mu}, \hat{\theta})}$$

μ parameter(s) of interest

θ profiled nuisance parameters

$L(\hat{\mu}, \hat{\theta})$ unconditional global likelihood maximum

$L(\mu, \hat{\hat{\theta}}(\mu))$ conditional maximum llh estimates for a given fixed value of μ

1. $-2\text{Ln}\Lambda(\mu)$ follows the χ^2 distribution with n dof, where n is the sum of the parameter of interests
2. $100(1-\alpha)\%$ CL defined by $-2\text{Ln}\Lambda(\mu) < k_\alpha$, where $P(\chi^2_n > k_\alpha) = \alpha$
3. PDF's used for the nuisance parameter are:
   - Gaussian (eg detector syst)
   - Poisson (eg uncert of number of events)
   - LogNormal (eg pdf not defined a priori)
4. Rectangular PDF's tested for a flat a priori likelihood in the range $\pm 1\sigma$ (eg tested in the mass measurement)

Log Likelihood Ratio

ATLAS-CONF-2013-040

10, 11]. A likelihood function $\mathcal{L}(\epsilon, \boldsymbol{\theta})$ with one parameter of interest is constructed as a product of conditional probabilities over the bins of the final discriminant in each channel (Eq. 1). The parameter of interest ϵ is defined as the fraction of $J^P = 0^+$ signal, such that $\epsilon = 1$ gives the Standard Model hypothesis, while $\epsilon = 0$ represents the $J^P = 2^+$ hypothesis. No *a priori* knowledge of the production cross sections or decay branching ratios is assumed. The number of signal events in each channel is a nuisance parameter in the likelihood:

$$\mathcal{L}(\epsilon, \boldsymbol{\theta}) = \prod_i^{N_{bins}} P(N_i | \epsilon \cdot S_i^{0^+}(\boldsymbol{\theta}) + (1-\epsilon) S_i^{2^+}(\boldsymbol{\theta}) + B_i(\boldsymbol{\theta})) \times \prod_j^{N_{sys}} \mathcal{A}(\tilde{\theta}_j | \theta_j)\,, \qquad (1)$$

where $\boldsymbol{\theta}$ represents all nuisance parameters. The likelihood function is a product of Poisson distributions P corresponding to the observation of N_i events in each bin i, given the models of the spin-0 and spin-2 signals and the backgrounds ($S_i^{0^+}(\boldsymbol{\theta})$, $S_i^{2^+}(\boldsymbol{\theta})$ and $B_i(\boldsymbol{\theta})$, respectively). Some of the nuisance parameters are constrained by auxiliary measurements through the functions $\mathcal{A}(\tilde{\theta}|\theta)$.

Test Statistic:

$$q = \log \frac{\mathcal{L}(\epsilon = 1, \hat{\hat{\theta}}_{\epsilon=1})}{\mathcal{L}(\epsilon = 0, \hat{\hat{\theta}}_{\epsilon=0})}\,,$$

The distribution of q is obtained using MC pseudo-experiments where the mean number of signal and bkg events is obtained from maximum llh fits to data. In the fits of each pseudo-exp. the number of signal and bkg events and all other NP are profiled

$$\mathrm{CL_s}(J^P = 2^+) = \frac{p_0(J^P = 2^+)}{1 - p_0(J^P = 0^+)}.$$

where the p_0 are obtained integrating the q distributions for the two hypothesis

Spin 2 model

For the $J^P = 2^+$ signal, the most general amplitude of the decay into two identical vector bosons contains 10 different terms and 10 effective coupling constants $g_{1..10}$ which are in general complex numbers [7]:

$$\begin{aligned} A(H \to VV) = \Lambda^{-1} \Big[& 2g_1 t_{\mu\nu} f^{*1,\mu\alpha} f^{*2,\nu\alpha} + 2g_2 t_{\mu\nu} \frac{q_\alpha q_\beta}{\Lambda^2} f^{*1,\mu\alpha} f^{*2,\nu\beta} \\ & + g_3 \frac{\tilde{q}^\beta \tilde{q}^\alpha}{\Lambda^2} t_{\beta\nu} (f^{*1,\mu\nu} f^{*2}_{\mu\alpha} + f^{*2,\mu\nu} f^{*1}_{\mu\alpha}) + g_4 \frac{\tilde{q}^\nu \tilde{q}^\mu}{\Lambda^2} t_{\mu\nu} f^{*1,\alpha\beta} f^{*(2)}_{\alpha\beta} \\ & + m_V^2 \left(2g_5 t_{\mu\nu} \epsilon_1^{*\mu} \epsilon_2^{*\nu} + 2g_6 \frac{\tilde{q}^\mu q_\alpha}{\Lambda^2} t_{\mu\nu} (\epsilon_1^{*\nu} \epsilon_2^{*\alpha} - \epsilon_1^{*\alpha} \epsilon_2^{*\nu}) + g_7 \frac{\tilde{q}^\mu \tilde{q}^\nu}{\Lambda^2} t_{\mu\nu} \epsilon_1^* \epsilon_2^* \right) \\ & + g_8 \frac{\tilde{q}_\mu \tilde{q}_\nu}{\Lambda^2} t_{\mu\nu} f^{*1,\alpha\beta} \tilde{f}^{*(2)}_{\alpha\beta} + g_9 t_{\mu\alpha} \tilde{q}^\alpha \epsilon_{\mu\nu\rho\sigma} \epsilon_1^{*\nu} \epsilon_2^{*\rho} q^\sigma \\ & + \frac{g_{10} t_{\mu\alpha} \tilde{q}^\alpha}{\Lambda^2} \epsilon_{\mu\nu\rho\sigma} q^\rho \tilde{q}^\sigma (\epsilon_1^{*\nu} (q\epsilon_2^*) + \epsilon_2^{*\nu} (q\epsilon_1^*)) \Big], \end{aligned} \tag{1}$$

where q, q_1 and q_2 denote the 4-momenta of the spin-2 particle and of vector bosons, respectively, and $\tilde{q} = q_1 - q_2$. The field strength tensor of the gauge boson with momentum q_i and polarisation ϵ_i is denoted $f^{(i),\mu\nu}$. The resonance wave function is given by a symmetric traceless tensor $t_{\mu\nu}$ and Λ is the mass scale associated with physics beyond the Standard Model.

The large number of free parameters in the couplings of a spin-2 particle makes it very difficult to exclude a generic spin-2 model. Instead, in this analysis a simple model is tested, namely a graviton-like tensor with minimal couplings, 2^+_m, where the only non-vanishing constants are $g_1 = g_5 = 1$. Two different production processes, $q\bar{q} \to H$ and $gg \to H$, are included for the 2^+_m model, with an arbitrary default $q\bar{q}$ fraction, $f_{q\bar{q}} = 25\%$. As will be discussed later, the analysis is performed for various values of $f_{q\bar{q}}$. Due to the lack of a definite prediction for the production cross section for 2^+_m events, the overall yield (proportional to cross section times branching ratio) of the signal events is fitted directly from the observed data.

[ATLAS-CONF-2013-031]